



**HAL**  
open science

## Development of molecularly imprinted polymer for the selective recognition of the weakly interacting fenamiphos molecule

Chaima Nasraoui, Najeh Jaoued-Grayaa, Laurent Vanoye, Yves Chevalier, Souhaira Hbaieb

### ► To cite this version:

Chaima Nasraoui, Najeh Jaoued-Grayaa, Laurent Vanoye, Yves Chevalier, Souhaira Hbaieb. Development of molecularly imprinted polymer for the selective recognition of the weakly interacting fenamiphos molecule. *European Polymer Journal*, 2022, 177, pp.111441. 10.1016/j.eurpolymj.2022.111441 . hal-03806439

**HAL Id: hal-03806439**

**<https://hal.science/hal-03806439>**

Submitted on 7 Oct 2022

**HAL** is a multi-disciplinary open access archive for the deposit and dissemination of scientific research documents, whether they are published or not. The documents may come from teaching and research institutions in France or abroad, or from public or private research centers.

L'archive ouverte pluridisciplinaire **HAL**, est destinée au dépôt et à la diffusion de documents scientifiques de niveau recherche, publiés ou non, émanant des établissements d'enseignement et de recherche français ou étrangers, des laboratoires publics ou privés.

# Development of molecularly imprinted polymer for the selective recognition of the weakly interacting fenamiphos molecule

Chaima Nasraoui<sup>1,3</sup>, Najeh Jaoued-Grayaa<sup>2</sup>, Laurent Vanoye<sup>4</sup>, Yves Chevalier<sup>3,\*</sup> and Souhaira Hbaieb<sup>1,\*</sup>

1- *Laboratoire de Recherche: Caractérisations, Applications et Modélisation de Matériaux, Université de Tunis El Manar, Faculté des Sciences de Tunis, Tunisia.*

2- *Unité Spécialisée de développement des techniques analytiques, Institut National de Recherche et d'Analyse Physico-chimique, Biotechpole Sidi-Thabet, 2020 Ariana, Tunisia.*

3- *Laboratoire d'Automatique, de Génie des Procédés et de Génie Pharmaceutique, LAGEPP, Université de Lyon 1, UMR 5007 CNRS, 43 bd 11 Novembre, 69622 Villeurbanne, France.*

4- *Catalyse, Polymérisation, Procédés et Matériaux, CP2M, Université de Lyon 1, CPE Lyon, UMR 5128 CNRS, 43 bd 11 Novembre, 69622 Villeurbanne, France.*

\* Corresponding authors:

Yves Chevalier: [yves.chevalier@univ-lyon1.fr](mailto:yves.chevalier@univ-lyon1.fr)

Tel: +33 472 431 877

Souhaira Hbaieb: [souhaira.hbaieb@fst.utm.tn](mailto:souhaira.hbaieb@fst.utm.tn)

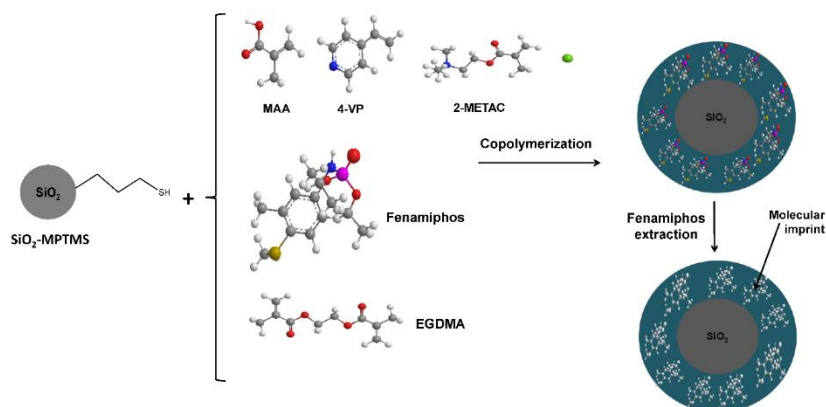
Tel: +216 98 94 74 79

Fax: +216 71 53 76 88

## Highlights

- Efficient MIP in spite of weak interactions with fenamiphos insecticide.
- MIPs as thin film onto modified silica surface for fenamiphos extraction.
- Adsorption behaviors of fenamiphos show the wide range of possible functional monomers.
- Quantitative assessment of MIPs adsorption isotherms by the Langmuir–Volmer model.

## Graphical abstract



## **Abstract**

The possible manufacture of Molecularly Imprinted Polymers (MIPs) under the conditions of weak interaction between the functional monomer and template molecule is addressed with the help of the case of the Fenamiphos organophosphorus insecticide. The choice of the functional monomer is addressed by investigating MIPs prepared by the surface imprinting technique using three very different types of monomers (methacrylic acid, 4-vinylpyridine and 2-(methacryloyloxyethyl)trimethylammonium chloride), a solid silica support grafted with 3-mercaptopropyltrimethoxysilane on its surface; ethylene glycol dimethacrylate as the cross-linker and acetonitrile as solvent. The prepared materials were characterized by IR, solid state  $^{13}\text{C}$  NMR, TGA, DLS, BET and TEM. Their performance as adsorbents were evaluated by modeling their experimental adsorption isotherms using the Langmuir–Volmer model. All MIPs show similar adsorbent performance although the functional monomers were quite different and the interactions with fenamiphos were weak. The latter were assessed by  $^1\text{H}$  and  $^{31}\text{P}$  NMR experiments in  $\text{DMSO-}d_6$  solution. The adsorption process presented weakly exothermic and endothermic behavior onto molecular imprints and non-specific sites respectively. The selectivity for adsorption of fenamiphos with respect to its sulfone and sulfoxide metabolites was quite high.

**Keywords:** Fenamiphos, Molecularly imprinted polymer; Adsorption; Modeling; Selectivity.

## 1. Introduction

Molecular imprinting technology is a trendy strategy widely used to design promising polymeric materials possessing specific cavities for a given target molecule. The concept of molecularly imprinted polymers (MIPs) is based on the copolymerization of a functional monomer and a cross-linking agent during which the template molecules bind to the functional monomer groups through non-covalent interactions. After completion of the polymerization, removal of the template molecules from the macromolecular matrix leaves cavities that are complementary to the template regarding their size, functional groups and shape [1]. Such “template-shaped cavities” known as molecular imprints of the template molecule are generated on MIPs surface and act as selective recognition site for adsorption of template molecules. As the preparation of MIPs is versatile, low-cost and simple, these materials are employed in various application fields such as selective solid phase adsorbents in the Solid phase extraction (SPE) technique [2]. Specifically, the analysis of compounds present in trace amounts in complex media (e.g. environment, food) requires a pre-treatment step of the collected sample to extract the analyte of interest from the matrix components and pre-concentrate it before its analysis by means of gas chromatography or high-performance liquid chromatography. Due to their high selectivity and affinity towards a target molecule, MIPs are suitable alternatives to the traditional SPE cartridges made of C18-grafted silica of poor selectivity.

The selection of a suitable functional monomer having favorable interactions with the template is crucial. It is often preferable to use a functional monomer possessing basic functional groups for acidic template and vice versa; e.g. methacrylic acid for basic template and vinylpyridine for acidic template [3].

Such selection is a difficult task when the template molecule does not include a functional group able to establish well-defined interactions with other molecules. The present work addresses this issue using fenamiphos as an illustrative example. Fenamiphos is an organophosphorus

insecticide whose chemical structure is given in Fig. 1. This molecule does not have clear-cut acidic or basic properties. On the one hand, a value of  $pK_a = 10.5$  has been reported [4], whereas on the other hand, it has been claimed that no  $pK_a$  value can be determined in water [5,6]. Its  $\text{Log}(P) = 3.3$  indicates medium polarity. Fenamiphos is an archetype of a molecule able to establish weak interactions only. Its complex chemical structure includes two weak basic groups and a weak acidic group that could be sites of interactions. For this reason, three very different types of monomers: acidic methacrylic acid (MAA), basic 4-vinylpyridine (4-VP) and cationic 2-(methacryloyloxyethyl)trimethylammonium chloride (2-METAC), were selected relying on the possible interactions that may occur with fenamiphos (Fig. 1) for a screening study of MIPs over a wide range of properties.

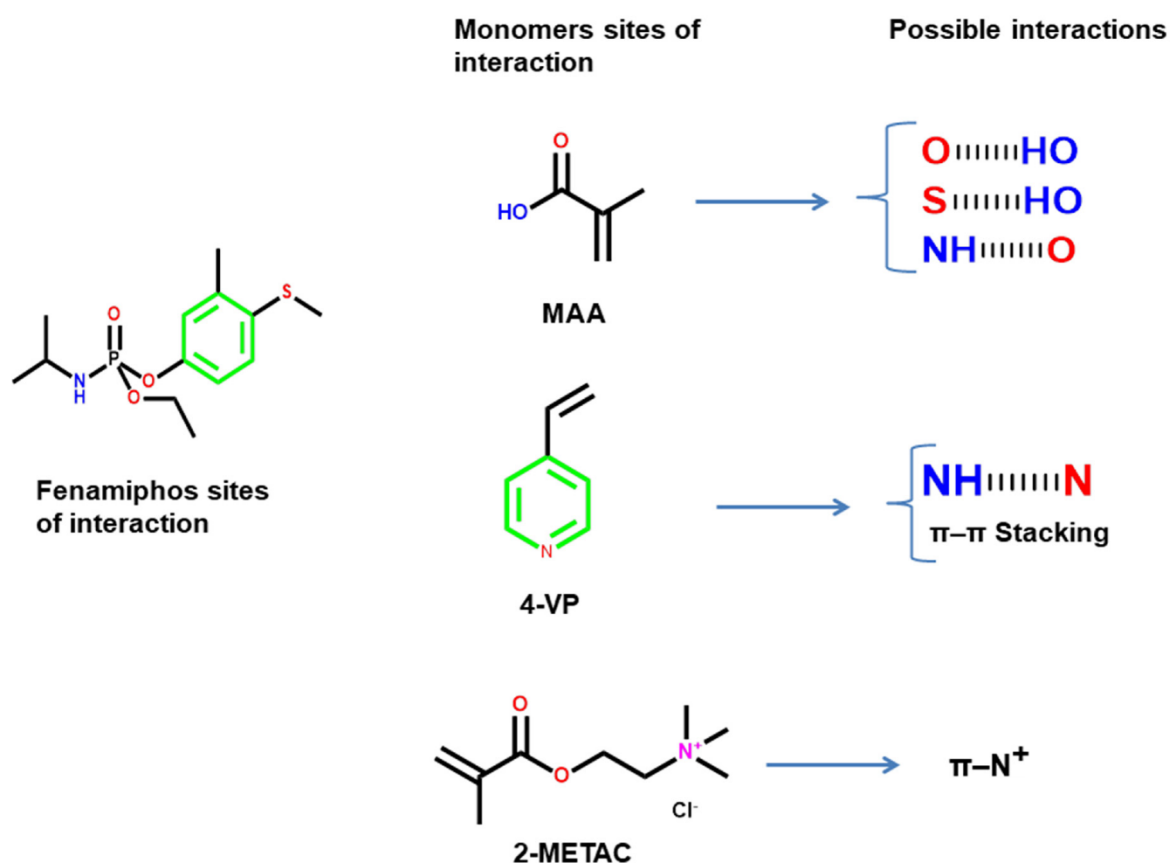


**Figure 1.** Possible interactions between fenamiphos and functional monomers.

The fenamiphos insecticide belongs to the organophosphorus class recognized by the World Health Organization as an extremely toxic class of chemicals. It is commonly used in every step of plant growth: pre-planting, at planting and pre- and post-harvest, and also to eradicate nematodes and thrips in agricultural soils [7]. Its inhibitory action of the acetylcholinesterase enzyme activity prevents hydrolysis of acetylcholine in the nervous system of a number of species, including humans [8]. The exposure of humans to fenamiphos from food or drinking water polluted with fenamiphos leads to chronic and acute toxicity. Hazardous effects have been noticed in aquatic and terrestrial organisms, particularly in fish and bird species. This is why, it is necessary to control its concentration in food, surface and groundwater.

The surface imprinting technique was used to prepare MIP for selective extraction of fenamiphos. This method limits many drawbacks of the conventional methods including low mass transfer, low binding rate, trapping of residual template [9–11]. MIP preparation strategy is outlined in Fig. 2. A solid support was made of fumed silica of high specific area. It was modified by grafting 3-mercaptopropyltrimethoxysilane so as to attach radical transferring groups (thiol groups) on its surface. EGDMA was used as the cross-linking agent to provide mechanical stability to the imprinted binding sites. The obtained materials were evaluated and compared by means of adsorption experiments including kinetics and equilibrium adsorption isotherms. The best material in terms of high capacity was further investigated in the thermodynamic study. Selectivity test towards fenamiphos mixed with its metabolites was performed for all the imprinted materials. Besides, the weak interactions between fenamiphos and every monomer in pre-polymerization mixture was studied in solution by NMR experiments.

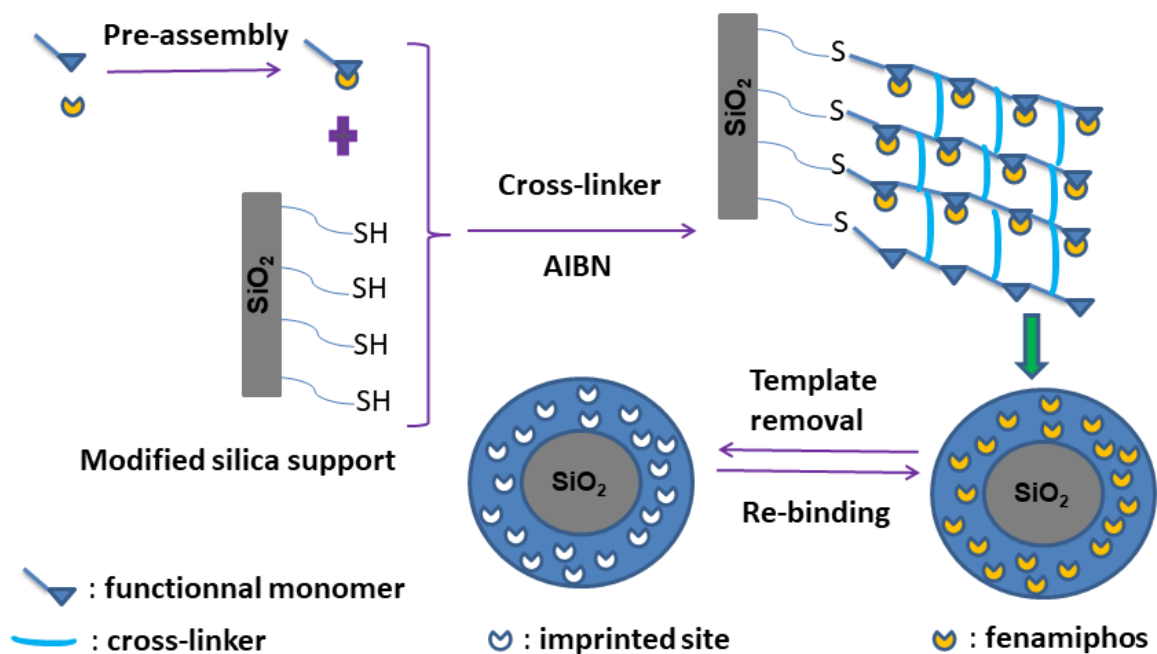


**Figure 2.** Schematic illustration of the synthetic route for the preparation of molecularly imprinted polymers.

## 2. Experimental section

### 2.1. Reagents

Fumed silica Cab-O-Sil with a mean size of primary particles of 7 nm and a specific area of  $200 \text{ m}^2 \cdot \text{g}^{-1}$  was purchased from Cabot Corporation and was dried at  $120 \text{ }^\circ\text{C}$  for 2 h under vacuum before use. 3-Mercaptopropyltrimethoxysilane (3-MPTMS, 95 %), methacrylic acid (MAA, 99 %), 4-vinylpyridine (4-VP, 95 %), 2-(methacryloyloxyethyl)trimethylammonium chloride (2-METAC, 85 %), azobisisobutyronitrile (AIBN), ethylene glycol dimethacrylate (EGDMA, 98 %) and N-ethyl-diisopropylamine ( $\geq 98 \text{ } \%$ ) were purchased from Sigma–Aldrich. Toluene was distilled before use. HPLC grade acetonitrile, methanol and tetrahydrofuran (THF) were purchased from Fisher Scientific. Fenamiphos ( $\geq 98 \text{ } \%$ ), fenamiphos sulfone ( $\geq 98 \text{ } \%$ ) and fenamiphos sulfoxide ( $\geq 98 \text{ } \%$ ) standards were provided from Sigma–Aldrich. Deuterated

dimethylsulfoxide (DMSO- $d_6$ ) used in NMR experiments was bought from Eurisotop (Saint-Aubin, France). Deionized water of 18 M $\Omega$ ·cm resistivity was used throughout the whole study.

## 2.2. Methods

Thermogravimetric analysis (TGA) were carried out on TG 209 F1 Netzsch instrument in the range of 25 °C to 1000 °C at a heating rate of 10 °C·min<sup>-1</sup> under a dynamic atmosphere of nitrogen. IR spectra were recorded with a Bruker IFS 55 Equinox FTIR spectrometer in ATR mode. The Raman spectra were recorded using a Jobin–Yvon T64000 spectrometer. Sulfur analyses were performed using a Perkin-Elmer CHS analyzer 2400 series II instrument. Solid-state <sup>13</sup>C NMR spectra were recorded on Bruker Avance III 500 ultra-shield PLUS spectrometer at 59.62 MHz. The particle sizes were determined by dynamic light scattering (DLS) using a Zetasizer Nano ZS instrument from Malvern Instruments (UK). The prepared materials were dispersed water with ultrasounds for 30 min and then analyzed by DLS in a polystyrene cuvette. The full nitrogen adsorption-desorption isotherms were performed at 77 K using a Micromeritics ASAP2020 instrument. Before nitrogen adsorption measurements, the MIPs were heated at 150 °C under vacuum. The Brunauer-Emmett-Teller (BET) method was used to calculate the specific surface area of MIPs. The porous volumes were calculated from the experimental desorption branch according to the Barret–Joyner–Halenda (BJH) method. Transmission Electron Microscopy (TEM) images were used to observe MIPs particles recorded on a Philips CM 120 microscope at 80 kV acceleration voltage at the “Centre Technologique des Microstructures” (CT $\mu$ ) (<http://microscopies.univ-lyon1.fr/>). Before TEM analysis, the samples were prepared by depositing a drop of 0.2 % aqueous dispersion on a Formvar film-coated grid then drying this droplet in the open air.

## 2.3. HPLC analyses

A HPLC system Agilent 1100 equipped with a DAD detector and a C18 column (100 mm × 4.6 mm, 2.6 μm) was used. The mobile phase consisted of methanol/water (80/20) used under isocratic condition. The injection volume was 10 μL, the flow rate was 0.8 mL·min<sup>-1</sup>, and the DAD detector was set at 250 nm wavelength. For selectivity experiment, the HPLC protocol was optimized to obtain a suitable separation between fenamiphos and its metabolites. A gradient elution program with a flow rate of 0.8 mL·min<sup>-1</sup> was used: acetonitrile/water (8/92) was kept for 2.5 min and changed to acetonitrile/water (60/40) in 23.5 min, kept constant for 2 min, and finally returned back to initial conditions within 2 min and maintained for 2 min to equilibrate the system. The injection volume was 10 μL and detection wavelength was set at 210 nm for fenamiphos sulfone, 240 nm for fenamiphos sulfoxide and 250 nm for fenamiphos.

#### **2.4. Preparation of the imprinted and non-imprinted materials**

A two-step procedure was adopted to prepare the imprinted polymers. First, the fumed silica was dried under a vacuum at 120 °C for two hours in order to remove adsorbed water. The surface of the dried silica was modified by grafting 3-MPTMS with anhydrous toluene as the solvent and N-ethyl-diisopropylamine as a catalyst. The reaction was run for 8 h at 110 °C under a nitrogen atmosphere. The resulting modified silica (SiO<sub>2</sub>-MPTMS) was filtered, thoroughly washed with THF and dried under vacuum at 60 °C. In the second step, 0.23 mmol of fenamiphos and 3.68 mmol of monomer were dissolved in 5 mL of acetonitrile. Then, 400 mg of SiO<sub>2</sub>-MPTMS was added and the mixture was deoxygenated with a nitrogen gas flow and heated to 70 °C. 4.6 mmol of EGDMA and 0.2 mmol of AIBN were then added to this mixture. The polymerization reaction proceeded for 2 h. The obtained material was filtered and washed with methanol to remove unreacted chemicals. The template molecules were washed off with methanol using a Soxhlet extractor. The extraction process continued until no more fenamiphos molecules were detected in the washing liquid by HPLC. Finally, the imprinted polymer (MIP) was dried under vacuum at 60 °C for 24 h. The corresponding non-imprinted polymer (NIP)

was also produced by following the above-described procedure but without the addition of fenamiphos. The several materials prepared by varying the type of monomer are summarized in [Table 2](#).

**Table 2.** Functional monomers used in the materials syntheses.

Monomer	Materials
Methacrylic acid	MIP/MAA NIP/MAA
2-(Methacryloyloxyethyl)trimethylammonium chloride	MIP/2-METAC NIP/2-METAC
4-Vinylpyridine	MIP/4-VP NIP/4-VP

## 2.5. Adsorption studies

### 2.5.1. Kinetic study

Kinetic studies were performed to study the effect of contact time on fenamiphos uptake and to determine the equilibrium time. The adsorption process was conducted for the time intervals of 5, 10, 25, 40 and 60 min at room temperature. The initial concentration of fenamiphos aqueous solution was fixed at  $350 \text{ mg}\cdot\text{L}^{-1}$ . 6 mg of each material was mixed with 3 mL of fenamiphos solution and the mixture was magnetically stirred at 500 rpm for different contact times of 5, 10, 25, 40 and 60 min at room temperature. Each aliquot was centrifuged for 10 min at 10000 rpm. The supernatant was filtered through a  $0.45 \mu\text{m}$  RC membrane and analyzed by HPLC. The adsorbed amount at time  $t$  ( $Q(t)$ ,  $\text{mg}\cdot\text{g}^{-1}$ ) was calculated using the following equation:

$$Q(t) = \frac{V}{m} [C(0) - C(t)] \quad (1)$$

where  $C(t)$  ( $\text{mg}\cdot\text{L}^{-1}$ ) is the residual fenamiphos concentration at time  $t$ ,  $C(0)$  is the initial fenamiphos concentration ( $\text{mg}\cdot\text{L}^{-1}$ ),  $V$  (L) is the volume of fenamiphos solution and  $m$  (g) is the mass of the adsorbent.

### 2.5.2. Adsorption isotherms

The static method was performed by mixing each prepared material (6 mg) with 3 mL of fenamiphos solution at different initial concentrations varied from 21 to 350 mg·L<sup>-1</sup> and at room temperature. The mixture was stirred for 60 min equilibration time, then centrifuged and filtered to measure the residual fenamiphos in the supernatant. The fenamiphos uptake at equilibrium defined as adsorption capacity  $Q_e$  (mol·m<sup>-2</sup>) was calculated using the following equation:

$$Q_e = \frac{V}{m A_{sp}} (C_i - C_e) \quad (2)$$

where  $C_i$  and  $C_e$  are the initial and equilibrium concentrations of fenamiphos solutions, respectively,  $V$  is the volume of fenamiphos solutions,  $m$  is the mass of the used material, and  $A_{sp}$  is the specific surface area of the material.

### 2.5.3. Adsorption isotherm modeling

The adsorption mechanism and affinity of the fenamiphos for the adsorbents were investigated through adsorption isotherms. The Langmuir–Volmer model [12] was used for its ability to model the simultaneous adsorption on and off the molecular imprints in MIPs. This model combines the localized selective (subscript S) adsorption process to molecular imprints (adsorption sites) described by the Langmuir model and the non-selective (subscript NS) adsorption as a mobile adsorbed layer (without well-defined sites) described by the Volmer model. The Volmer model was used to describe fenamiphos adsorption onto non-imprinted polymers.

The following equations define the Volmer and Langmuir models respectively:

$$C = \frac{1}{K_{NS}} \frac{\theta}{1-\theta} e^{\frac{\theta}{1-\theta}} \quad (3)$$

where  $\theta$  is the surface coverage,  $\theta = \frac{Q_{NS}}{Q_{max,NS}}$  and  $K_{NS}$  is the binding constant for adsorption equilibrium.

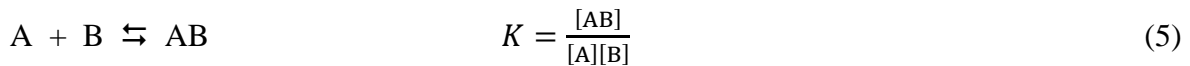
$$Q_S = Q_{\max,S} \frac{K_S C}{1 + K_S C} \quad (4)$$

where  $C$  is the equilibrium concentration of fenamiphos adsorbate.  $Q_{\max,S}$  is the maximum adsorption capacity.  $K_S$  is the Langmuir constant related to the standard free energy of adsorption.

#### 2.5.4. NMR study

$^1\text{H}$  and  $^{31}\text{P}$  NMR experiments were performed in  $\text{DMSO-}d_6$  solution to determine the association constants ( $K$ ) of fenamiphos and the functional monomers (MAA, METAC, 4-VP). Fenamiphos and monomer were mixed in various proportions varying from 90/10 to 8/92 at a fixed concentration of fenamiphos ( $[A]_{\text{total}} = 0.11 \text{ mol}\cdot\text{L}^{-1}$ ).  $^1\text{H}$  and  $^{31}\text{P}$  NMR spectra were recorded on a Bruker AV500 spectrometer at 500 MHz and 202 MHz respectively. The association constants were determined by non-linear regression of 1:1 association model to experimental chemical shifts.

The 1:1 association model is described by a simple equilibrium where fenamiphos (noted A) and a monomer (noted B) associate together into a new species noted AB



The mass balances of A and B read

$$[\text{A}]_{\text{total}} = [\text{A}] + [\text{AB}] \quad (6)$$

$$[\text{B}]_{\text{total}} = [\text{B}] + [\text{AB}] \quad (7)$$

In the fast exchange limit, the observed chemical shift of each  $^1\text{H}$  or  $^{31}\text{P}$  NMR line of fenamiphos ( $\delta$ ) is the weighted average of the chemical shifts of the free ( $\delta_A$ ) and associated molecules ( $\delta_{AB}$ ).

$$\delta = \frac{[\text{A}]}{[\text{A}]_{\text{total}}} \delta_A + \frac{[\text{AB}]}{[\text{A}]_{\text{total}}} \delta_{AB} \quad (8)$$

Solving [Eq. 5](#) together with the mass balance [Eqs 6](#) and [7](#) yields

$$[AB] = \frac{1}{2} \left[ [A]_{\text{total}} + [B]_{\text{total}} + \frac{1}{K} - \sqrt{\left( [A]_{\text{total}} + [B]_{\text{total}} + \frac{1}{K} \right)^2 - 4[A]_{\text{total}}[B]_{\text{total}}} \right] \quad (9)$$

### 2.5.5. Competitive binding experiments

Fenamiphos metabolites such as fenamiphos sulfone and fenamiphos sulfoxide are chosen as competing species in the adsorption experiments to explore the molecular imprinting effect of the MIP materials. These molecules were selected due to their similar structure and their high frequency of occurrence together with fenamiphos in the environmental matrix such as groundwater or soil. Aqueous solutions containing  $100 \text{ mg}\cdot\text{L}^{-1}$  of fenamiphos, fenamiphos sulfone and fenamiphos sulfoxide were prepared. The experiment was performed by mixing 6 mg of the adsorbent with 3 mL of the prepared mixture. After stirring for 60 min at 500 rpm and at room temperature, the supernatant was separated and analyzed by HPLC. The extraction efficiencies *EE* of fenamiphos and its analogs from the solution onto the used adsorbents were calculated from the equilibrium concentration  $C_e$  measured in the supernatant and the initial concentration of analyte ( $C_i$ ) as:

$$\text{Extraction Efficiency (\%): } EE = \frac{100}{C_i} (C_i - C_e) \quad (10)$$

Through the parameters outlined in Eqs. 11 and 12, the distribution coefficient ( $D$ ,  $\text{L}\cdot\text{g}^{-1}$ ) and the selectivity coefficient ( $\alpha$ ) were determined to evaluate the selectivity of adsorbent. The distribution coefficient for each substance was expressed as the ratio of the adsorption capacity of the adsorbent at equilibrium to the concentration of adsorbate remaining in solution at equilibrium.

$$D = \frac{Q_e}{C_e} \quad (11)$$

The selectivity coefficient  $\alpha$  was calculated according to Eq. 12:

$$\alpha = \frac{D_{\text{analyte,MIP}}}{D_{\text{competitor,MIP}}} \quad (12)$$

where  $D_{\text{analyte,MIP}}$  and  $D_{\text{competitor,MIP}}$  are the distribution coefficients for the template molecule and for the competitive molecules respectively.

### 3. Results and discussion

#### 3.1. Synthesis and characterization of imprinted materials

The silica support was firstly chemically grafted with 3-MPTMS in order to attach thiol groups that are strong radical transfer agents in the radical polymerization. The grafting process performed in anhydrous toluene yields a dense monomolecular layer of organosilane attached to the silica surface [10,13]. The resulting SiO<sub>2</sub>-MPTMS particles were characterized by IR spectroscopy, Raman scattering, <sup>13</sup>C CP-MAS NMR, thermogravimetric analysis and sulfur elemental analysis. The results are given in the [Supporting Information](#).

The type of polymerization plays an important role to prepare a good selective imprinted polymer. The surface imprinting polymerization method was selected because of its many advantages compared to the traditional bulk polymerization method. In fact, the use of this technique can increase the molecular recognition ability between polymers and target molecule during adsorption process due to the presence of the imprinting sites on the outer layer of polymer based on substrate, improve the mass transfer kinetics and avoid incomplete template removal. Among the different surface imprinting techniques, grafting polymerization synchronized with cross-linking imprinting has been employed as a polymerization strategy ([Fig. 2](#)). It is based on two processes: (1): fenamiphos and the monomer are combined beforehand to interact and to form a pre-polymerization complex. (2): the thiol group bound to the surface of SiO<sub>2</sub>-MPMTS and the added initiator form the initiation system to induce monomer-fenamiphos complexes and cross-linking EGDMA to produce graft cross-linking copolymerization, generating a layer of copolymer on the surface of modified silica and fenamiphos molecules, trapped in the cross-linked networks. Moreover, a self-assembly

approach for molecular imprinting was utilized which is based on non-covalent interactions between template and monomer such as hydrogen bond, hydrophobic and van der Waals forces. It is the most widely used strategy for imprinted polymers manufacturing because it is easier in template-monomer complex preparation, easier in template removal and produce imprinted polymers with high-affinity binding [14]. The choice of appropriate functional monomer is essential. It allows the formation of a stable template-monomer complex in the pre-polymerization stage and builds template specific sites in the polymer imprinting process. This choice is difficult in the case of fenamiphos because this molecule does not have clear-cut physicochemical properties. The fenamiphos molecule possesses nitrogen, oxygen and sulfur atoms that can be involved in hydrogen bonds and an aromatic ring that can form interactions involving its  $\pi$ -electrons. MAA is a widely employed acidic functional monomer, which has been selected because of its ability to act as both a hydrogen bond acceptor and a donor. Besides, two other types of monomer were also chosen, basic one such as 4-VP possessing the H-bond accepting property of the pyridine nitrogen and a cationic one 2-METAC containing quaternary ammonium group which can form cation- $\pi$  interactions with the fenamiphos aromatic ring. Acetonitrile was a suitable solvent because it is able to promote non-covalent interactions without interfering with the radical polymerization [15]. In all cases, the imprinted and non-imprinted materials were characterized by means of IR spectroscopy, solid-state  $^{13}\text{C}$  CP/MAS NMR, TGA and BET measurements. IR spectra of the imprinted and their corresponding non-imprinted polymers display similar characteristic bands (Fig. 3 and Fig. S4). This result suggests that these polymers contained similar chemical compositions that would be expected due to the similarity in their polymerization components. The IR spectra of MIP/MAA and NIP/MAA (Fig. 3) show a band at  $2900\text{ cm}^{-1}$  ascribed to the C-H stretching vibrations present in EGDMA and MAA, a band at  $1723\text{ cm}^{-1}$  belonging to the stretching vibration of C=O in MAA and EGDMA, bands at  $1458\text{ cm}^{-1}$  and  $1388\text{ cm}^{-1}$  assigned to the bending vibrations of

C–H in  $-\text{CH}_3$  and  $-\text{CH}_2$ , and a band at  $950\text{ cm}^{-1}$  attributed to the C–O stretching. The disappearance of the characteristic S–H stretching band of the thiol at  $2576\text{ cm}^{-1}$  also revealed that the radical transfer reactions during polymerization converted the thiol groups to completion. Hence, it is clear that MAA was successfully cross-linked through EGDMA to the surface of  $\text{SiO}_2$ -MPTMS. The same conclusions were reached for materials based on 2-METAC and 4-VP (Fig. S4).

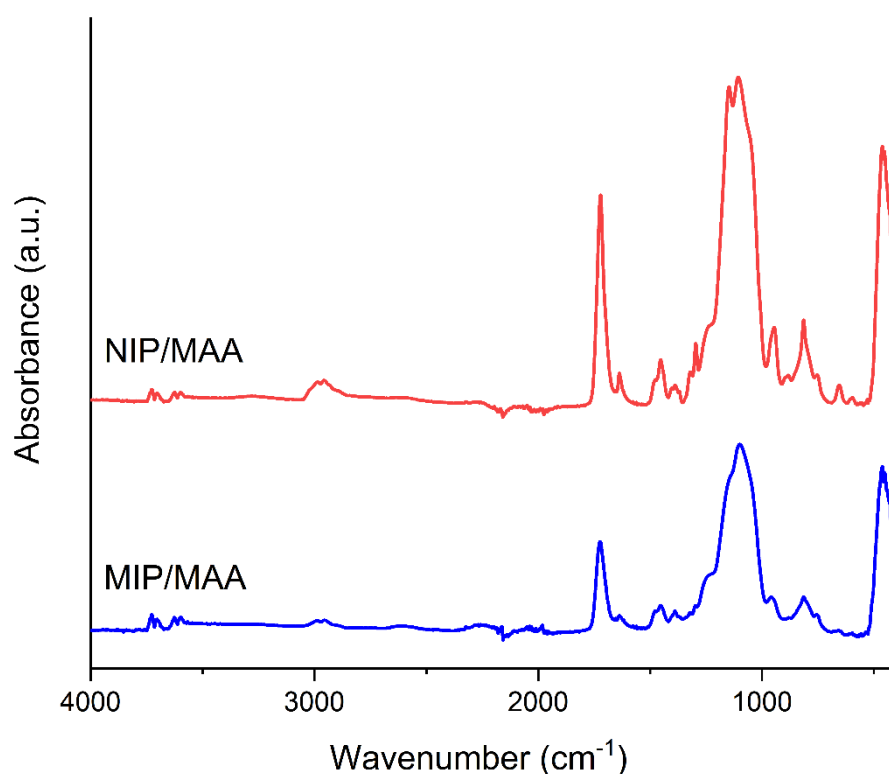


**Figure 3.** IR spectra of MIP/MAA and NIP/MAA.

The solid-state  $^{13}\text{C}$  NMR spectra of all MIPs and NIPs revealed similar signals (Fig. 4 and Fig. S5) suggesting that carbon atoms have identical arrangement in the polymeric network. As expected, this confirms the chemical equivalence of MIP and NIP prepared from the same reagents. Signals belonging to methyl ( $-\text{CH}_3$ ), methylene ( $-\text{CH}_2-\text{O}-$ ) and carbonyl ( $-\text{O}-\text{C}=\text{O}$ ) groups are observed in all spectra at around 4 ppm, 49 ppm and 165 ppm respectively. In addition, a strong resonance observed in the aliphatic region (31 ppm) is related to the cross-

linking agent and functional monomers (CH<sub>2</sub>). A signal at nearly 124 ppm is attributed to the residual unreacted double bonds. MIP/2-METAC and NIP/2-METAC spectra exhibit supplementary strong signal at 40 ppm corresponding to carbon atoms of the quaternary ammonium group. Therefore, this result indicates that all observed resonances are in good agreement with the expected composition of the materials and provide complete proof for the successful copolymerization on the modified silica surface.

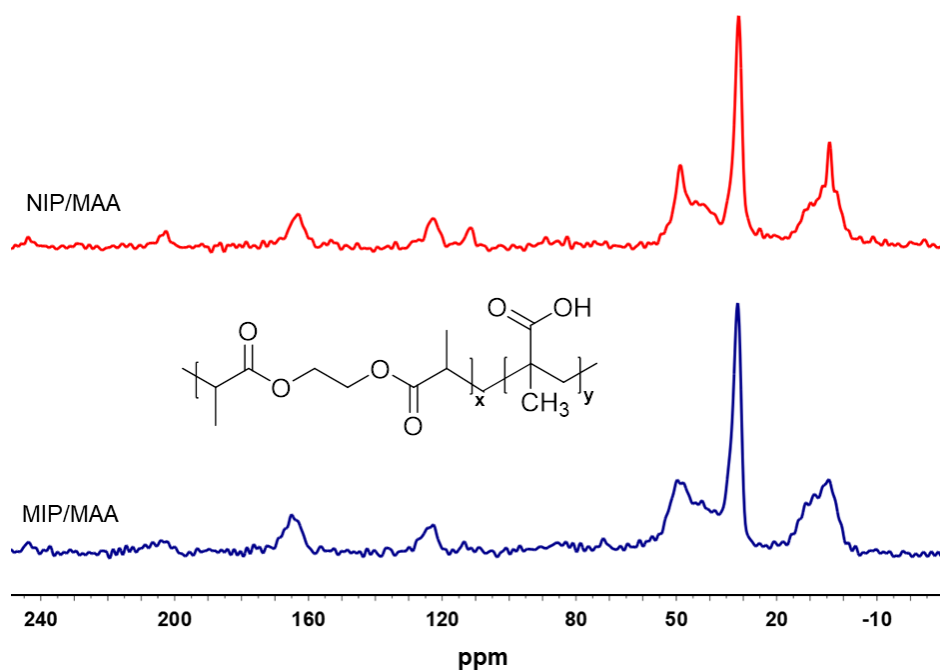


**Figure 4.** Solid-state <sup>13</sup>C CP/MAS NMR spectra of the materials: MIP/MAA and NIP/MAA materials.

Thermogravimetric analysis was used for the determination of the grafting density. In all cases, the imprinted and non-imprinted materials had similar TGA patterns (Fig. 5 and Fig. S6). A first step of almost 10 % mass loss was observed in the temperature range of 100–200 °C related to the release of adsorbed water. The second stage is a large mass loss in the range 250–450 °C is due to the thermal decomposition of the polymer coatings. The decomposition of the polymer material occurs in several successive steps for MIP/2-METAC and NIP/2-METAC (Fig. S6).

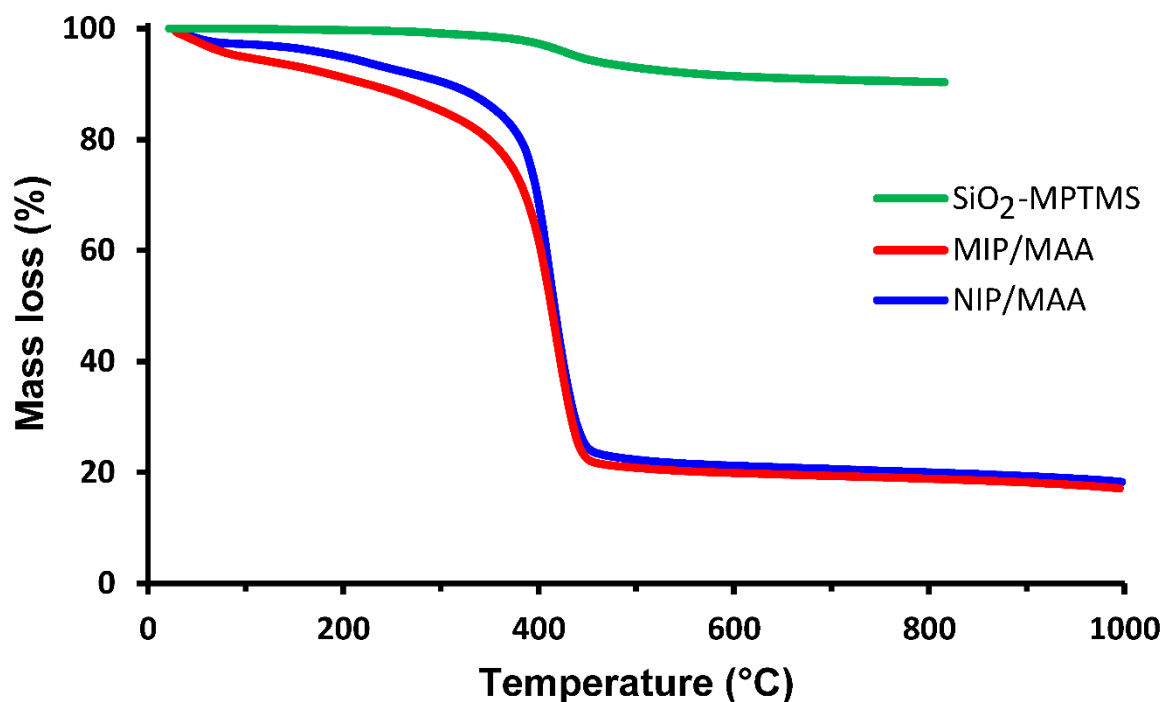


**Figure 5.** Thermogravimetric analysis of SiO<sub>2</sub>-MPTMS, MIP/MAA and NIP/MAA.

The grafting densities were calculated using Eq. 13:

$$\text{grafting density} = \frac{M(\text{copolymer}) - M(\text{modified silica})}{100 \times M_{\text{mol}}(\text{grafted copolymer})} \quad (13)$$

where  $M(\text{copolymer})$  is the mass loss of copolymer,  $M(\text{modified silica})$  is the mass loss of modified silica, and  $M_{\text{mol}}(\text{grafted copolymer})$  is the molar mass of the average repeat units of grafted monomer/cross-linker 50/50 copolymer.  $M_{\text{mol}}(\text{grafted copolymer}) = 284.28 \text{ g}\cdot\text{mol}^{-1}$  for MIP/MAA,  $303.36 \text{ g}\cdot\text{mol}^{-1}$  for MIP/4-VP and  $405.92 \text{ g}\cdot\text{mol}^{-1}$  for MIP/2-METAC.

The grafting densities for all the prepared materials were similar (Table 3). As expected, the imprinted polymers and their non-imprinted counterpart have the same density because they are prepared by the same reagents. In case of materials prepared by MAA as monomer, the grafting densities are slightly higher due to the high reactivity of MAA in radical polymerization. These values are similar to those reported in the literature [16].

**Table 3.** Characteristics of the materials: Mass loss relative to the dry material from TGA and corresponding grafting density, and size of the materials dispersed in water as measured by DLS.

Materials	Mass loss (%)	Grafting density (mmol·g <sup>-1</sup> )	Particle size from TEM (nm)	Aggregate size from DLS (nm)
SiO <sub>2</sub> -MPTMS	7.0	0.94		173
MIP/MAA	79.1	2.8	16.5 ± 1.3	664
NIP/MAA	80.5	2.8	(SD = 4.4 nm)	779
MIP/2-METAC	69.4	1.7	20.4 ± 1.0	220
NIP/2-METAC	69.5	1.7	(SD = 3.6 nm)	353
MIP/4-VP	71.5	2.4	26.2 ± 1.5	794
NIP/4-VP	71.5	2.4	(SD = 5.3 nm)	648

TEM was used to investigate MIPs morphology. TEM micrographs of the three MIPs (Fig. 6) revealed quite similar morphologies. Small primary particles of nearly spherical shape had sizes ranging from 15 nm to 25 nm. Image analysis gave their mean diameter and the standard deviation of the size distribution given in Table 3. Such primary particles were strongly agglomerated, as it is often the case with small-sized nanoparticles that have been dried and redispersed. The fumed silica support was already aggregated before operating the grafting processes (Fig. 6a,b). It is made clear that the morphology of the materials was dictated by that of the silica support SiO<sub>2</sub>-MPTMS.

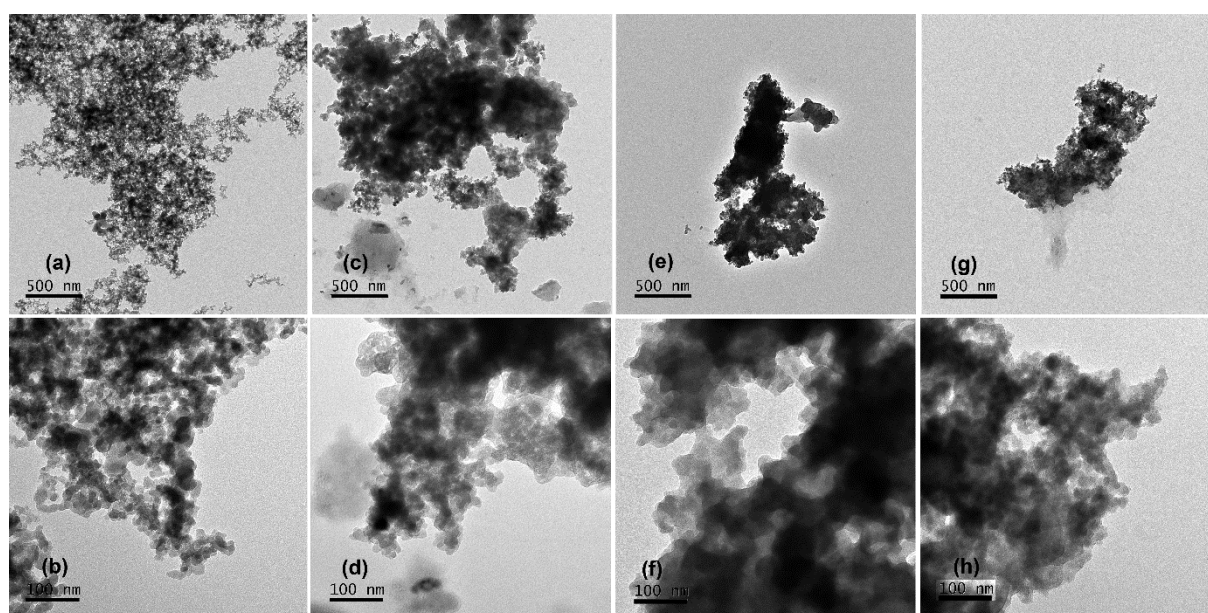


**Figure 6.** TEM images at two magnifications of SiO<sub>2</sub>-MPTMS (a,b), MIP/MAA (c,d), MIP/4-VP (e,f) and MIP/2-METAC (g,h).

The BET measurements of nitrogen gas adsorption at 77 K were used to evaluate the specific surface area and the porosity of MIPs. The adsorption-desorption isotherms of nitrogen gas are shown in Fig. 7. The adsorption isotherms of the three MIPs had similar profiles with a hysteresis between the adsorption and desorption branches and no clear final saturation plateau as the pressure approaches the saturated vapor pressure of nitrogen ( $p_0$ ). These isotherms are not matching a definite type of the IUPAC classification [17]; their features are intermediate between types II and IV. The type IV is characterized by the presence of mesopores of size in the 10–100 nm range causing capillary condensation of nitrogen and a hysteresis at desorption. The BET specific surface area was  $A_{SP} = 60 \text{ m}^2 \cdot \text{g}^{-1}$  for MIP/MAA,  $A_{SP} = 81 \text{ m}^2 \cdot \text{g}^{-1}$  for MIP/2-METAC and  $A_{SP} = 80 \text{ m}^2 \cdot \text{g}^{-1}$  for MIP/4-VP. These values were lower than that of the functional silica support  $\text{SiO}_2\text{-MPTMS}$  ( $150 \text{ m}^2 \cdot \text{g}^{-1}$ ) showing that the copolymerization of the monomer and the cross-linker onto  $\text{SiO}_2\text{-MPTMS}$  caused a loss of specific area. These results suggested that elementary silica particles were partly buried (encapsulated) by the polymer coating. The interstices in between them were partly filled and a part of the specific area of  $\text{SiO}_2\text{-MPTMS}$  was lost. The BET specific surface areas were the same for MIP/2-METAC and MIP/4-VP, and slightly lower for MIP/MAA. This result indicates that the monomer type does not have a significant effect on the distribution of the polymer coating during the polymerization in acetonitrile. The mesoporosity was analyzed by the BJH method on the desorption branches although the isotherms were clearly not of type IV (Fig. 7). The total (cumulated) porous volume was  $0.2 \text{ cm}^3 \cdot \text{g}^{-1}$  (~20 %) for MIP/MAA,  $0.33 \text{ cm}^3 \cdot \text{g}^{-1}$  (~33 %) for MIP/4-VP and  $0.29 \text{ cm}^3 \cdot \text{g}^{-1}$  (~29 %) for MIP/2-METAC. Such porous volumes were quite low, in accordance with the weak hysteresis of the adsorption isotherms. The mesoporous volume of the starting silica support was quite large  $1.5 \text{ cm}^3 \cdot \text{g}^{-1}$  because the silica material is made of aggregated primary particles of about 20 nm diameter. The aggregates have a low density because of the large voids between primary particles that correspond to the large mesoporous volume. Both the lower

specific surface area of the MIP compared to the starting silica support and the weak hysteresis of the BET data indicate a low mesoporosity and adsorption behavior that better corresponds to the type II of the IUPAC classification already observed in previous works [16]. The loss of mesoporous volume after polymerization indicate that the polymer material filled the mesopores of the silica support, which has already been inferred from the loss of specific area.

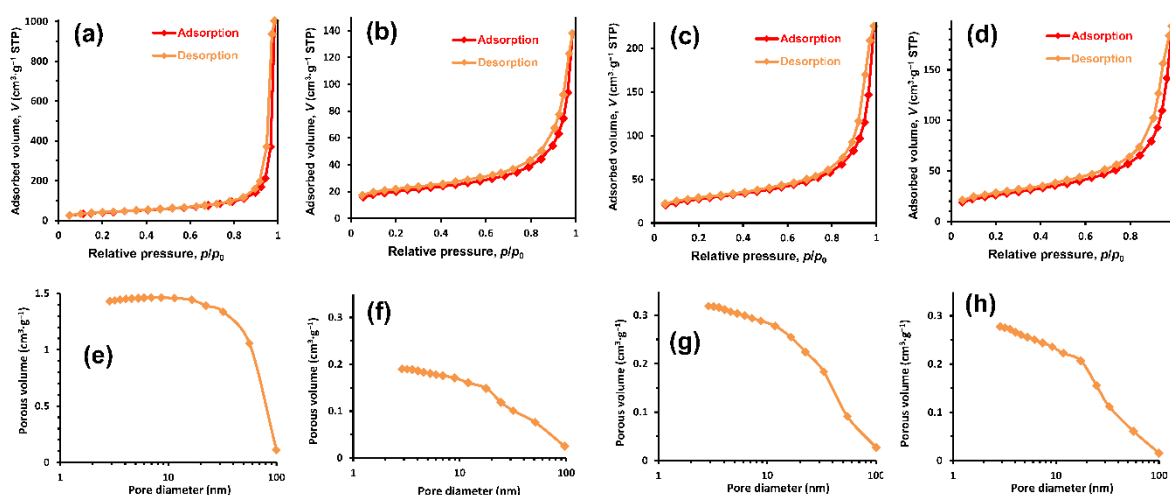


**Figure 7.** BET adsorption (red) and desorption (orange) isotherms of nitrogen gas at 77 K (a, b, c and d) and cumulated volume assessed by the BJH method (e, f, g and h) for SiO<sub>2</sub>-MPTMS (a,e), MIP/MAA (b,f) and MIP/4-VP (c,g) and MIP/2-METAC (d,h).

The state of nanoparticles in aqueous suspension was investigated by measuring the hydrodynamic size of their aggregates by DLS (Table 3). All MIP and NIP materials had larger sizes than SiO<sub>2</sub>-MPTMS, which feature shows that the coating process by the polymer material caused a supplementary aggregation of silica. The type of functional monomer had a definite influence on the measured sizes, in agreement with previous literature reports [18]. The size of materials based on 2-METAC was close to (slightly larger) that of the starting SiO<sub>2</sub>-MPTMS silica, probably because of the efficient stabilization by the permanent electrical charge of the quaternary ammonium group of 2-METAC generates strong repulsive interactions in the polar

solvent medium of polymerization (acetonitrile). On the contrary, the materials based on MAA or 4-VP as functional monomers hardly ionize in the aprotic acetonitrile medium.

### **3.2. Performance of the imprinted materials**

The main criterion for assessing performance is the adsorption behavior. The depletion method was used to measure the adsorbed amounts of solute from its aqueous solution to the solid particles of MIP and NIP. The difference of adsorbed amounts between the MIP and NIP materials is considered as an evidence for the presence of molecular imprints [1]. Fast adsorption kinetics is a mandatory specification of many applications in the field of analytical chemistry. Equilibrium adsorption isotherms allow for a thermodynamic approach of interactions “at” and “off” the molecular imprints. The properties of materials based on various functional monomers can be quantitatively compared.

#### **3.2.1. Adsorption kinetics**

The design of the materials consists in a thin polymer coating grafted at the surface of a porous solid support made of fumed silica. This surface MIP technology ensures a high accessibility to the molecular imprints. Therefore, adsorption kinetics were fast. The adsorption kinetics (Fig. 8) could be split into two phases: fast adsorption lasting less than 5 min, and subsequent slower adsorption thereafter. A plateau indicating equilibrium adsorption was reached within 20 min. The initial fast adsorption process accounted for approximately 80% (MIP/MAA and MIP/4-VP) to 100% (MIP/2-METAC) of the full adsorption. The fast kinetics were mainly ascribed to the imprinted coating layer and the high silica specific surface area that greatly shortens diffusion time [19]. This result is consistent an interesting comparative study in which the imprinted polymer prepared by surface layer imprinting showed rapid kinetic for gossypol adsorption upon reaching saturation at  $t = 40$  min while the imprinted polymer prepared by the traditional bulk polymerization presented very slow adsorption kinetics where reaching equilibrium required 720 min [20]. Such rapid mass transfer rate is advantageous for use in

sample pre-concentrations by solid phase extraction (SPE) leading to a shorter duration of analyses. Moreover, it was noticed that the adsorption on imprinted materials is as fast as that on non-imprinted ones because kinetics is controlled by the morphology of the starting silica support. In all cases, fenamiphos adsorption capacities of imprinted polymers are higher than that of their corresponding non-imprinted ones.

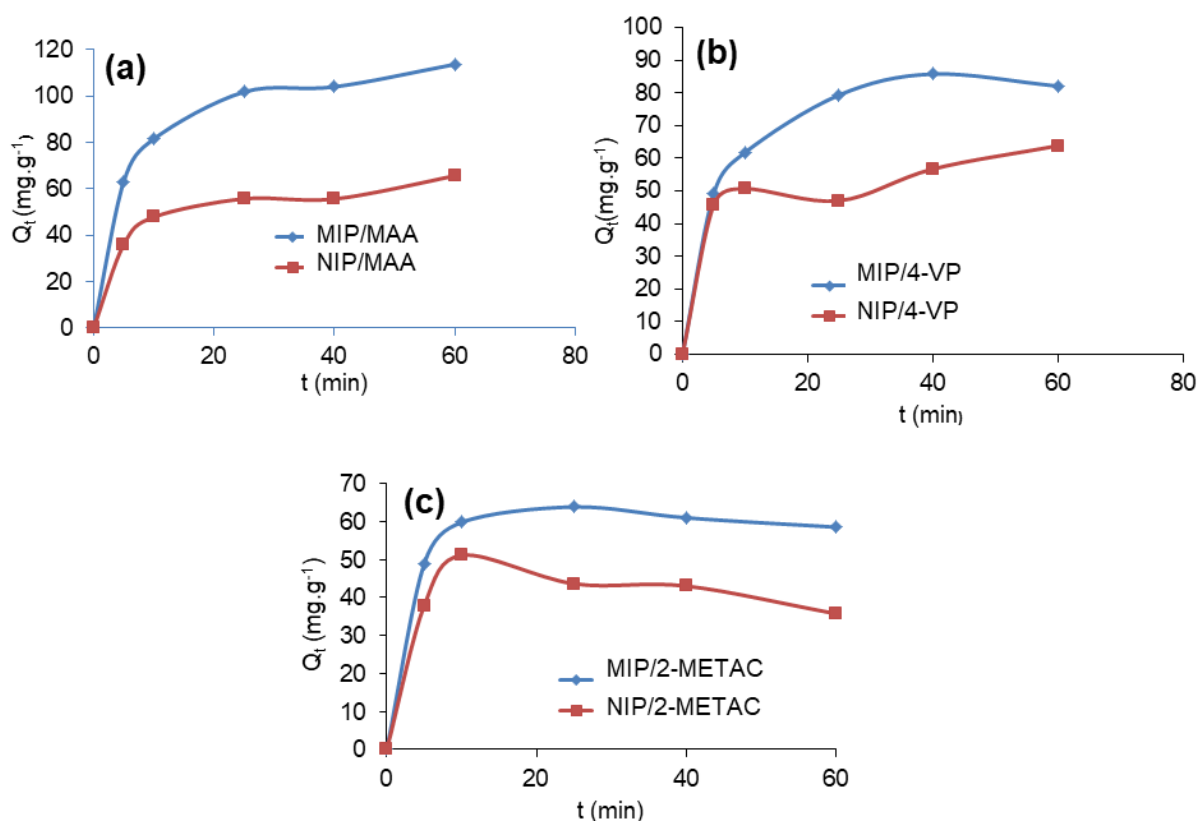


**Figure 8.** Effect of contact time on adsorption capacity of fenamiphos onto: (a): MIP/MAA and NIP/MAA, (b): MIP/4-VP and NIP/4-VP, (c): MIP/2-METAC and NIP/2-METAC at 25 °C.

### 3.2.2. Adsorption isotherms

Equilibrium adsorption isotherms of MIPs and NIPs have been measured for all materials over a wide concentration range for adsorption models could be fitted to the experimental data. Fig. 9 shows the adsorption isotherms of fenamiphos on MIP and NIP materials. All the isotherms have the same classical shape. The adsorbed amount of fenamiphos increases with increasing initial concentration and reaches a plateau for the largest concentrations at which all the

adsorption sites are occupied and the whole surface area is covered by adsorbed fenamiphos molecules. Concentrations above  $350 \text{ mg}\cdot\text{L}^{-1}$  were not investigated due to the limited solubility of fenamiphos in water. In all cases, the amount of fenamiphos bound to the MIP is higher than to the NIP, showing that imprinted sites were indeed generated on the surface of these materials in addition to the surface available for non-specific adsorption. Thermodynamic models were fitted to the adsorption data in order to obtain the parameters describing the adsorption equilibrium. Even the simplest adsorption process is described by two independent parameters, a binding constant and a maximum adsorbed amount. Visual examination of experimental adsorption isotherm is somehow a vain endeavor because it is difficult to figure out whether higher adsorption capacity of the material comes from a stronger affinity or a larger density of molecular imprints. A higher affinity comes from stronger interactions, whereas a higher capacity comes from a higher surface density of adsorption sites or a larger available surface area. The use of models is necessary in order to compare materials properties in a quantitative manner. The Langmuir isotherm model was used to describe adsorption on localized molecular imprints, and the Volmer isotherm model was utilized for non-selective mobile (non-localized) adsorption beside the molecular imprints [12]. The adsorbed molecules are mobile and diffuse laterally on the surface in case of non-localized binding. Such adsorption can be described by Volmer model because it fits the physicochemical mechanism of non-selective adsorption as a layer of mobile adsorbed molecules. The Scatchard plots frequently used to assess the adsorption behavior are not accurate to calculate binding constants and  $Q_{\max}$  because the underlying model is a Langmuir-type adsorption on well-defined localized sites. However, Scatchard plots clearly revealed at a qualitative level two kinds of “binding sites” on the MIP surface indicating its heterogeneity, and only one kind of “binding site” on the NIP surface [21–24]. Thus, the adsorption on MIP was presently modeled using the Langmuir–Volmer adsorption isotherm and adsorption on NIP was modeled using the Volmer adsorption (Fig. 9)

[12]. The theoretical adsorption isotherms were fitted to the experimental data by minimizing the average relative error function (*ARE*):

$$ARE = \frac{1}{n-p} \sum_{i=1}^n \left| \frac{Q_{exp} - Q_{calc}}{Q_{exp}} \right| \quad (10)$$

with  $n$  and  $p$  are the number of data points and fitted parameters respectively,  $Q_{exp}$  and  $Q_{calc}$  are the experimental and fitted adsorption capacities at equilibrium respectively.

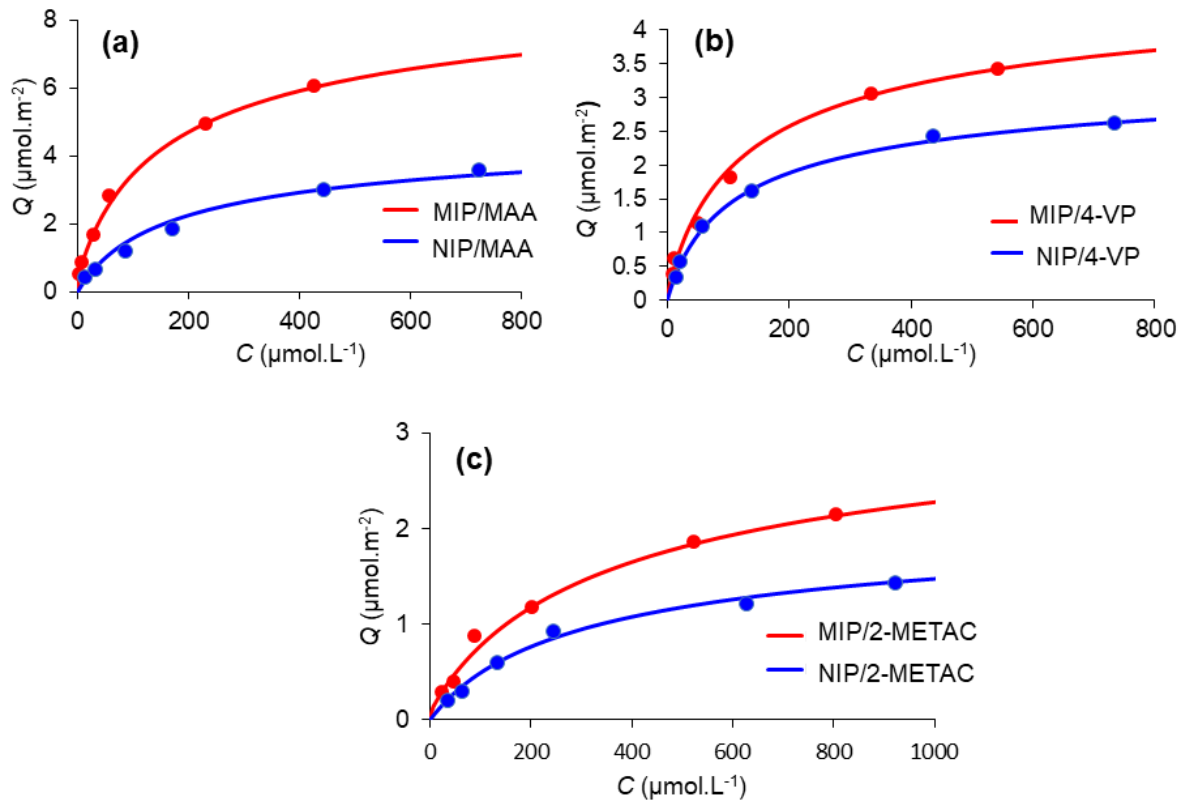


**Figure 9.** Experimental adsorption isotherms and best non-linear fits of the adsorption models for adsorption of fenamiphos onto: (a): MIP/MAA and NIP/MAA, (b): MIP/4-VP and NIP/4-VP, (c): MIP/2-METAC and NIP/2-METAC at 25 °C.

The parameters  $Q_{max,NS}$  and  $K_{NS}$  of the Volmer isotherm are related to the non-specific adsorption. Specific adsorption on molecular imprints is described by the parameters of Langmuir isotherm  $Q_{max,S}$  and  $K_S$ . *ARE* values and the parameters of Langmuir and Volmer isotherms are tabulated in Table 4. Fig. 9 shows that the adsorption models fit very well the

experimental adsorption isotherms and it is confirmed by the low values of *ARE*. The most striking feature is that all of the three very different functional monomers were able to provide selective molecular imprints. Among the materials, MIP/MAA had the best molecular binding ability for fenamiphos. It exhibits the highest adsorption capacity ( $Q_{\max,S} + Q_{\max,NS}$ ) and the highest  $Q_{\max,S}$  even though MIP/MAA had a slightly lower BET specific surface area than the other MIPs. This is because the hydrogen bonding interaction between fenamiphos and MAA may be formed between the sulfur and oxygen atoms of fenamiphos and the carboxylic acid group of MAA. In the case of 4-VP, hydrogen bond can occur with the nitrogen of pyridine and the weakly basic N–H group of fenamiphos, together with other possible weak interactions like  $\pi$ - $\pi$  and van der Waals. Finally for 2-METAC, a cation- $\pi$  interaction can occur between the quaternary ammonium of 2-METAC and the aromatic ring of fenamiphos. All these interactions between fenamiphos and functional groups of the polymer material seems being weak and close in term of strength owing to the  $K_S$  values for the three MIPs. The equilibrium constants  $K_S$  (to molecular imprints of MIPs) are much higher than the  $K_{NS}$  (to NIPs) for all materials showing a much higher affinity to molecular imprints than for the non-selective adsorption. In all cases, a difference between  $Q_{\max,NS}$  (MIP) and  $Q_{\max,NS}$  (NIP) is observed (Table 4). This may be explained by the fact that there are selective sites that have been damaged during the extraction of the template or/and during grinding and the crushing step converting specific adsorption sites into non-specific adsorption areas. To conclude, there is a wide range of possible functional monomers allowing the preparation of MIPs binding weakly interactive molecules. The MIP technology nevertheless creates selective molecular imprints. The MIP/MAA material was the best selective adsorbent compared to the MIP/2-METAC and the MIP/4-VP. It showed higher adsorption capacity and stronger adsorption onto the molecular imprints. MIP/MAA has been taken for an investigation of the enthalpic and entropic contributions to the free energy of adsorption through measurements of the temperature dependence of adsorption isotherms.

**Table 4.** Parameters of the best fits of the Volmer and Langmuir–Volmer models to experimental adsorption isotherms of fenamiphos onto NIP and MIP materials at 298 K.

Materials	Non-selective adsorption		Selective adsorption		ARE
	$Q_{\max,NS}$ ( $\mu\text{mol}\cdot\text{m}^{-2}$ )	$\log(K_{NS})$	$Q_{\max,S}$ ( $\mu\text{mol}\cdot\text{m}^{-2}$ )	$\log(K_S)$	
NIP/MAA (Volmer)	6.69	3.62	–	–	0.18
MIP/MAA (Langmuir–Volmer)	12.17	3.66	0.451	6.09	0.14
NIP/4-VP (Volmer)	4.59	3.84	–	–	0.08
MIP/4-VP (Langmuir–Volmer)	6.34	3.78	0.115	5.83	0.24
NIP/2-METAC (Volmer)	3.08	3.36	–	–	0.060
MIP/2-METAC (Langmuir–Volmer)	4.76	3.29	0.098	5.71	0.13

### 3.2.3. Thermodynamic study

A thermodynamic study of fenamiphos adsorption isotherms was applied on MIP/MAA by varying the temperature (298 K, 303 K, 313 K and 323 K). The recorded adsorption isotherms at different temperatures presented in Fig. 10a show that the adsorbed amount slightly decreased with respect to increasing temperature. The reason may be that the higher the temperature, the faster and the stronger the movement of molecules making up the fenamiphos molecules to adsorbed from adsorbent sites into the solution.

The standard Gibbs free energy  $\Delta_{\text{ads}}G^0$ , enthalpy  $\Delta_{\text{ads}}H^0$  and entropy  $\Delta_{\text{ads}}S^0$  listed in Table 5 are calculated from the binding constant ( $K_S$  and  $K_{NS}$ ) determined at different temperatures and from the slope and the intercept of van't Hoff plot (Fig. 10b) for specific and non-specific binding sites ( $i = S$  or  $NS$ ). These thermodynamic parameters were determined to gain an idea about the thermodynamic behavior of the adsorption process.

The van't Hoff equation is as follows:

$$\ln(K_i) = \frac{\Delta_{\text{ads}}S_i^0}{R} - \frac{\Delta_{\text{ads}}H_i^0}{RT} \quad (11)$$

The linearity of plots shown in Fig. 10b confirms the independence of adsorption with the tested temperature range. The value of  $\Delta_{\text{ads}}G^0$  for adsorption to selective sites is higher than that to non-selective areas, which is a direct consequence of the  $K_S$  and  $K_{NS}$  values. The negative value of  $\Delta_{\text{ads}}H^0$  for selective sites and a positive value of  $\Delta_{\text{ads}}H^0$  for non-selective adsorption show an exothermic nature of adsorption to molecular imprints and an endothermic behavior of the adsorption process beside molecular imprints. The nature of adsorption, which can be physical or chemical, is provided by the absolute value of  $\Delta_{\text{ads}}H^0$ . In this case, the absolute value of  $\Delta_{\text{ads}}H^0$  was lower than  $40 \text{ kJ}\cdot\text{mol}^{-1}$  suggesting that the adsorption of fenamiphos onto both molecular imprints and non-selective areas is mainly physical adsorption [30]. The negative value of  $\Delta_{\text{ads}}H^0$  teaches that the transfer of fenamiphos from solution to selective sites of MIP is enthalpically favored. Meanwhile, the positive value of  $\Delta_{\text{ads}}H^0$  may be due to the dehydration of the non-selective areas in MIP.

Standard entropy changes  $\Delta_{\text{ads}}S^0$  provide information about the disorder degree of the interface between the adsorbent binding sites and the adsorbate in solution before and after adsorption.  $\Delta_{\text{ads}}S_S^0$  and  $\Delta_{\text{ads}}S_{NS}^0$  were found positive, indicating an increase in randomness of adsorbate-solution interface during the adsorption process and replacement of water molecules by fenamiphos inside the cavity of molecular imprints and non-selective ones. The non-similarity between  $\Delta_{\text{ads}}S_S^0$  and  $\Delta_{\text{ads}}S_{NS}^0$  values reveals a difference in the adsorption behavior of fenamiphos on each type of site may be due to the difference in affinity of fenamiphos towards specific and non-specific sites.

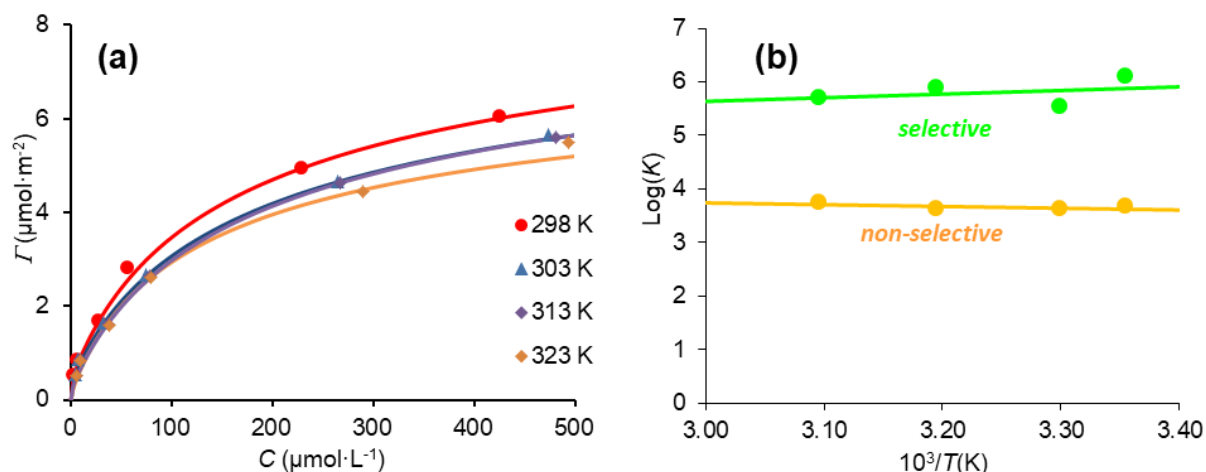


**Figure 10.** (a): Effect of temperature on the fenamiphos adsorption onto MIP/MAA and (b): van't Hoff plot of the binding constant of fenamiphos onto MIP/MAA against inverse temperature.

**Table 5.** Thermodynamic parameters for selective and non-selective adsorption of fenamiphos onto MIP/MAA at 298 K.

Adsorption sites	$\Delta_{\text{ads}}H^0$ ( $\text{kJ}\cdot\text{mol}^{-1}$ )	$\Delta_{\text{ads}}S^0$ ( $\text{J}\cdot\text{mol}^{-1}\cdot\text{K}^{-1}$ )	$\Delta_{\text{ads}}G^0$ ( $\text{kJ}\cdot\text{mol}^{-1}$ )
Selective site	-13.0	69.0	-34.7
Non-selective site	6.4	90.9	-20.9

### 3.3. NMR study of fenamiphos-monomer associations

It is considered that the first step for the successful formation of molecular imprints is the association of the template molecule and functional monomer as a “pre-polymerization complex”. Hence, the selection of the functional monomer may be based on an assessment of such interactions in solution in the polymerization medium.

Such interaction can be investigated by experimental tools (e.g. NMR) or can be predicted by theoretical chemistry calculations [25,26]. Therefore, the intermolecular fenamiphos/monomer interactions have been evaluated in DMSO-*d*<sub>6</sub> solution by a <sup>1</sup>H and <sup>31</sup>P NMR study of the chemical shifts variations in fenamiphos/monomer mixtures of different compositions. The variations of chemical shifts as a function of the [monomer]/[fenamiphos] ratio are shown in Figs S7, S8 and S9 in Supporting Information. In all cases, <sup>1</sup>H signals were shifted downfield

as the concentration of the monomer increases indicating a deshielding effect upon complexation [27]. For the case of fenamiphos/MAA interaction, the HD, HK lines of protons in vicinity of the oxygen atom and HE in vicinity of the NH group showed the most noticeable chemical shift variations (Fig. S8). This is suggesting the formation of hydrogen bonds between fenamiphos oxygen atom and OH group of the MAA carboxylic acid, and also hydrogen bond between fenamiphos NH group and the carbonyl group of MAA. In fenamiphos/2-METAC interaction, large shift changes were observed for the aromatic protons HA, HB and HC, which may be due to  $N^+-\pi$  interactions between the quaternary ammonium group of fenamiphos and the aromatic ring of fenamiphos. Finally in the case of fenamiphos/4-VP interaction, the chemical shift changes were high for the aromatic protons (HA, HB and HC) and HE in vicinity of NH group, indicating a combination of  $\pi-\pi$  interaction and hydrogen bond between the nitrogen atom and fenamiphos NH group. Furthermore, the measured chemical shifts did not reach a plateau, even for a large excess of monomer, showing that complexation of fenamiphos did not reach completion in the concentration range studied. This clearly indicates that the complex is weakly associated. This result was confirmed by the low association constant values inferred by modeling the association process (Table 6). Strikingly, the results of adsorption kinetics and isotherms demonstrated the generation of imprints on MIPs surface although the associations of fenamiphos and the monomers were weak. The template-monomer association strength only provides a clue for selecting the most favorable functional monomer. These are actually the interactions with the growing chains of polymer material that matter. Indeed, potentially all components present during the polymerization reaction can participate in complexation of the template [28]. The present work shows that MIPs with high selectivity and affinity could be obtained whereas the strengths of the template/monomer associations were weak in pre-polymerization mixtures with association constants ranging between 1 and 10. This result can be attributed to the formation of three-dimensional polymer network that trap the

template molecules by stiffening the polymer structure around the template molecule and freezing its molecular imprints [29].

**Table 6.** Association constants of the complexes between fenamiphos and the monomers in DMSO-*d*<sub>6</sub>.

Complex system	Association constants
Fenamiphos/MAA	$0.70 \pm 0.001$
Fenamiphos/METAC	$0.60 \pm 0.001$
Fenamiphos/4-VP	$0.34 \pm 0.003$

### 3.5. Selectivity

Selectivity expresses by the ability of an adsorbent to differentiate and quantify the analyte of interest in the presence of other interfering molecules possessing a similar structure. It is based on binding sites configuration and functional groups orientation in the binding sites. Selectivity is a crucial criterion to evaluate the recognition properties of imprinted polymers. For this purpose, fenamiphos metabolites were chosen as potential competitors for adsorption in a selectivity trial. Their molecular structures are given in Fig. 11. The characteristic parameters  $D$  and  $\alpha$  of the competitive adsorption calculated from Eqs 11 and 12 are presented in Table 7. The distribution coefficient of fenamiphos in all MIPs was obviously higher than the distribution coefficients of its competitors and it is more pronounced in the case of MIP/MAA. The imprinted polymers exhibit remarkably higher extraction efficiency of the target molecule than its structural analogs. This kind of site created on imprinted polymer surface enables to distinguish template molecules through their shape, functional group distribution and size. In addition, the results showed that all polymers have good selectivity towards fenamiphos with the presence of its metabolites. The extraction efficiency of fenamiphos by MIP/MAA was higher than that obtained by the other materials. Low extraction efficiency of both interfering compounds by the prepared polymers was observed because these molecules can be adsorbed

onto the non-selective sites, and may also be recognized by the imprinted cavities, but to a lesser extent than the template molecule. In fact, the competing molecules are closely related to fenamiphos in terms of structural similarity and molar mass; but they are differentiated by the presence of sulfone or sulfoxide groups. In all cases, the values of selectivity coefficient  $\alpha$  with respect to fenamiphos were high. Such a result demonstrates the high selective recognition of the imprinted polymer towards fenamiphos indicating that the imprinted cavities created by the template are not able to accommodate fenamiphos sulfone and fenamiphos sulfoxide. This may be due to the higher polarity of the interferents and to the presence of additional basic oxygen atoms. The distribution coefficients of fenamiphos metabolites obtained from their adsorption onto MIP/MAA were higher than MIP/2-METAC and MIP/4-VP. On the basis of the original view stating that the selectivity comes from the shape-recognition by a rigid cavity, fenamiphos and its metabolites should bind in a similar manner. However, selectivity also relies on interactions between functional groups of the adsorbing molecules and well-positioned and oriented groups at the binding sites [30]. The latter mechanism may make a predominant contribution to the selectivity.  $^1\text{H}$  NMR measurements of the interactions of fenamiphos and the functional monomers have shown that the sulfide group of fenamiphos was one of the interaction sites, so that it was not surprising that its substitution by sulfone or sulfoxide impaired the selectivity.

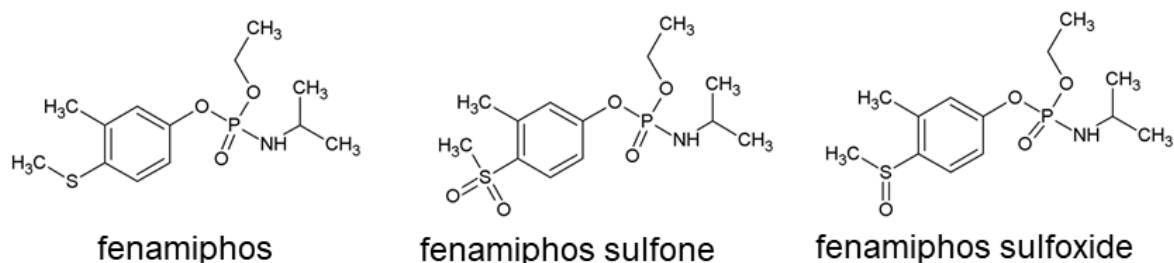


**Figure 11.** Chemical structures of fenamiphos and its metabolites.

**Table 7.** Extraction efficiencies, distribution coefficients ( $D$ ) and selectivity coefficients ( $\alpha$ ) of imprinted materials.

Molecules	MIP/MAA			MIP/2-METAC			MIP/4-VP		
	$EE$ (%)	$D$ ( $L \cdot g^{-1}$ )	$\alpha$	$EE$ (%)	$D$ ( $L \cdot g^{-1}$ )	$\alpha$	$EE$ (%)	$D$ ( $L \cdot g^{-1}$ )	$\alpha$
Fenamiphos	81.0	2.14	–	38.6	0.31	–	66.7	1	–
Fenamiphos sulfone	26.0	0.18	12	7.8	0.042	7	17.7	0.11	9
Fenamiphos sulfoxide	10.3	0.06	36	2.8	0.014	22	3.2	0.02	50

#### 4. Conclusion

The preparation of molecularly imprinted polymers was achieved through surface molecular imprinting method using functionalized silica nanoparticles as solid support. Three functional monomers of very different natures (MAA, 2-METAC and 4-VP) were investigated. All of them show weak interactions with the fenamiphos molecule in solution. They allowed the formation of molecular imprints to comparable extents. MAA is by far the most used functional monomer [31], including for extraction of pesticides (organophosphorus diazinon, quinalphos and chlorpyrifos in fruit samples [32], ziram dithiocarbamate fungicide [33]). Owing to the present results, the predominant use of MAA as a functional monomer may be questioned.

The adsorption kinetics of the different materials were fast; adsorption equilibrium was reached within 20 min. The Langmuir–Volmer model fitted well the experimental adsorption isotherms of imprinted polymers, while the adsorption onto their non-imprinted counterparts was in agreement with the Volmer model that takes into consideration the mobility of the adsorbate for non-specific adsorption. MIP/MAA exhibited the highest adsorption capacity, possessed monodispersed particles and its thermodynamic study revealed that the adsorption onto selective sites was exothermic and onto non-selective binding sites was endothermic. Surprisingly, high selectivity performance was achieved with the three functional monomers, even though the interactions between fenamiphos and these monomers were weak. Overall, MIP/MAA can be selected again as an adsorbent in the SPE technique to selectively extract

fenamiphos from complex media and generate an enrich extraction medium to be used for quantitative analysis.

## Acknowledgments

This work was supported by the “PHC Utique” program for French-Tunisian cooperation (project number 19G1204).

## References

- [1] B. Sellergren, (ed.), *Molecularly Imprinted Polymers. Man-made Mimics of Antibodies and their Applications in Analytical Chemistry*. Elsevier, Amsterdam (2001).
- [2] A.G. Mayes, K. Mosbach, Molecularly imprinted polymers: useful materials for analytical chemistry? *Trends Anal. Chem.* 16 (1997) 321–332. doi:[10.1016/S0165-9936\(97\)00037-X](https://doi.org/10.1016/S0165-9936(97)00037-X)
- [3] L.I. Andersson, K. Mosbach, Enantiomeric resolution on molecularly imprinted polymers prepared with only non-covalent and non-ionic interactions. *J. Chromatogr. A* 516 (1990) 313–322. doi:[10.1016/S0021-9673\(01\)89273-6](https://doi.org/10.1016/S0021-9673(01)89273-6)
- [4] National Library of Medicine (2004). NIH.  
<https://chem.nlm.nih.gov/chemidplus/rn/22224-92-6>
- [5] K.A. Lewis, J. Tzilivakis, D. Warner, A. Green, An international database for pesticide risk assessments and management. *Hum. Ecol. Risk Assess. (HERA)* 22 (2016) 1050–1064. doi:[10.1080/10807039.2015.1133242](https://doi.org/10.1080/10807039.2015.1133242)
- [6] Fenamiphos (85) - Food and Agriculture Organization.  
[https://www.fao.org/fileadmin/templates/agphome/documents/Pests\\_Pesticides/JMPR/Evaluation99/15Fenamiphos.pdf](https://www.fao.org/fileadmin/templates/agphome/documents/Pests_Pesticides/JMPR/Evaluation99/15Fenamiphos.pdf)
- [7] G.N. Agrios, Control of plant diseases, in: *Plant Pathology*, G.N. Agrios (ed.), Academic Press, San Diego, 9 (2005) 293–353. doi:[10.1016/B978-0-08-047378-9.50015-4](https://doi.org/10.1016/B978-0-08-047378-9.50015-4)
- [8] T. Cáceres, M. Megharaj, K. Venkateswarlu, N. Sethunathan, R. Naidu, Fenamiphos and related organophosphorus pesticides: Environmental fate and toxicology. In: D.M. Whitacre (ed.), *Rev. Environ. Contamin. Toxicol.* 205 (2010) 117–162. doi:[10.1007/978-1-4419-5623-1\\_3](https://doi.org/10.1007/978-1-4419-5623-1_3)

- [9] P. Ma, Z. Zhou, W. Xu, T. Fan, W. Yang, Preparation of surface molecularly imprinted polymers for selective removal and determination of sulphamethoxazole from aqueous media. *Adsorption Sci. Technol.* 33 (2015) 45–62. doi:[10.1260/0263-6174.33.1.45](https://doi.org/10.1260/0263-6174.33.1.45)
- [10] C. Ayadi, A. Anene, R. Kalfat, Y. Chevalier, S. Hbaieb, Molecularly imprinted polyaniline on silica support for the selective adsorption of benzophenone-4 from aqueous media. *Colloids Surfaces A: Physicochem. Eng. Aspects* 567 (2019) 32–42. doi:[10.1016/j.colsurfa.2019.01.042](https://doi.org/10.1016/j.colsurfa.2019.01.042)
- [11] C. Dong, H. Shi, Y. Han, Y. Yang, R. Wang, J. Men, Molecularly imprinted polymers by the surface imprinting technique. *Eur. Polym. J.* 145 (2021) 110231. doi:[10.1016/j.eurpolymj.2020.110231](https://doi.org/10.1016/j.eurpolymj.2020.110231)
- [12] C. Ayadi, A. Anene, R. Kalfat, Y. Chevalier, S. Hbaieb, Molecular imprints frozen by strong intermolecular interactions in place of cross-linking. *Chem. Eur. J.* 27 (2021) 2175–2183. doi:[10.1002/chem.202004580](https://doi.org/10.1002/chem.202004580)
- [13] N. Jaoued-Grayaa, C. Nasraoui, Y. Chevalier, S. Hbaieb. Design of molecularly imprinted polymer materials relying on hydrophobic interactions. *Colloids Surfaces A: Physicochem. Eng. Aspects* 647 (2022) 129008. doi:[10.1016/j.colsurfa.2022.129008](https://doi.org/10.1016/j.colsurfa.2022.129008)
- [14] A.N. Hasanah, N. Safitri, A. Zulfa, N. Neli, D. Rahayu, Factors affecting preparation of molecularly imprinted polymer and methods on finding template-monomer interaction as the key of selective properties of the materials. *Molecules* 26 (2021) 5612. doi:[10.3390/molecules26185612](https://doi.org/10.3390/molecules26185612)
- [15] A. Binsalom, I. Chianella, K. Campbell, M. Zourob, Development of solid-phase extraction using molecularly imprinted polymer for the analysis of organophosphorus pesticides-(chlorpyrifos) in aqueous solution. *J. Chromatogr. Sep. Tech.* 7 (2016) 1000340. doi:[10.4172/2157-7064.1000340](https://doi.org/10.4172/2157-7064.1000340)
- [16] A. Anene, R. Kalfat, Y. Chevalier, S. Hbaieb, Design of molecularly imprinted polymeric materials: The crucial choice of functional monomers. *Chem. Africa* 3 (2020) 769–781. doi:[10.1007/s42250-020-00180-1](https://doi.org/10.1007/s42250-020-00180-1)
- [17] M. Thommes, K. Kaneko, A.V. Neimark, J.P. Olivier, F. Rodriguez-Reinoso, J. Rouquerol, K.S.W. Sing, Physisorption of gases, with special reference to the evaluation of surface area and pore size distribution (IUPAC Technical Report). *Pure Appl. Chem.* 87 (2015) 1051–1069. doi:[10.1515/pac-2014-1117](https://doi.org/10.1515/pac-2014-1117)
- [18] K. Yoshimatsu, T. Yamazaki, I.S. Chronakis, L. Ye, Influence of template/functional monomer/cross-linking monomer ratio on particle size and binding properties of

- molecularly imprinted nanoparticles. *J. Appl. Polym. Sci.* 124 (2012) 1249–1255. doi:[10.1002/app.35150](https://doi.org/10.1002/app.35150)
- [19] H. Zhou, K. Peng, Y. Su, X. Song, J. Qiu, R. Xiong, L. He, Preparation of surface molecularly imprinted polymer and its application for the selective extraction of teicoplanin from water. *RSC Adv.* 11 (2021) 13615–13623. doi: [10.1039/d1ra00913c](https://doi.org/10.1039/d1ra00913c)
- [20] L. Wang, K. Zhi, Y. Zhang, Y. Liu, L. Zhang, A. Yasin, Q. Lin, Molecularly imprinted polymers for gossypol via sol-gel, bulk, and surface layer imprinting-A comparative study. *Polymers* 11 (2019) 602. doi:[10.3390/polym11040602](https://doi.org/10.3390/polym11040602)
- [21] B. Zu, G. Pan, X. Guo, Y. Zhang, H. Zhang, Preparation of molecularly imprinted polymer microspheres via atom transfer radical precipitation polymerization, *J. Polym. Sci., Part A: Polym. Chem.* 47 (2009) 3257–3270. doi:[10.1002/pola.23389](https://doi.org/10.1002/pola.23389)
- [22] B. Zu, Y. Zhang, X. Guo, H. Zhang, Preparation of molecularly imprinted polymers via atom transfer radical “bulk” polymerization, *J. Polym. Sci., Part A: Polym. Chem.* 48 (2010) 532–541. doi:[10.1002/pola.23750](https://doi.org/10.1002/pola.23750)
- [23] Y. Ma, G. Pan, Y. Zhang, X. Guo, H. Zhang, Comparative study of the molecularly imprinted polymers prepared by reversible addition–fragmentation chain transfer “bulk” polymerization and traditional radical “bulk” polymerization, *J. Mol. Recogn.* 26 (2013) 240–251. doi:[10.1002/jmr.2267](https://doi.org/10.1002/jmr.2267)
- [24] K. Nian, L. Zheng, X. Cheng, Preparation of molecularly imprinted polymers for recognition and extraction of benzoylureas from apple samples. *Polymer-Plastics Technol. Mater.* 59 (2020) 1204–1217. doi:[10.1080/25740881.2020.1719146](https://doi.org/10.1080/25740881.2020.1719146)
- [25] I.A. Nicholls, S. Chavan, K. Golker, B.C.G. Karlsson, G.D. Olsson, A.M. Rosengren, S. Suriyanarayanan, J.G. Wiklander, Theoretical and computational strategies for the study of the molecular imprinting process and polymer performance. In: B. Mattiasson, L. Ye (eds.), *Molecularly Imprinted Polymers in Biotechnology, Advances in Biochemical Engineering/Biotechnology*. Springer Cham, (2015) pp. 25–50. doi:[10.1007/10\\_2015\\_318](https://doi.org/10.1007/10_2015_318)
- [26] B. Qader, I. Hussain, M. Baron, R. Jimenez-Perez, J. Gonzalez-Rodriguez, G. Gil-Ramírez, A molecular imprinted polymer sensor for biomonitoring of fenamiphos pesticide metabolite fenamiphos sulfoxide. *Electroanalysis* 33 (2021) 1129–1136. doi:[10.1002/elan.202060599](https://doi.org/10.1002/elan.202060599)
- [27] Q. Osmani, H. Hughes, P. McLoughlin, Probing the recognition of molecularly imprinted polymer beads. *J. Mater. Sci.* 47 (2012) 2218–2227. doi:[10.1007/s10853-011-6032-4](https://doi.org/10.1007/s10853-011-6032-4)

- [28] B.C.G. Karlsson, J. O'Mahony, J.G. Karlsson, H. Bengtsson, L.A. Eriksson, I.A. Nicholls, Structure and dynamics of monomer-template complexation: An explanation for molecularly imprinted polymer recognition site heterogeneity. *J. Am. Chem. Soc.* 131 (2009) 13297–13304. doi:[10.1021/ja902087t](https://doi.org/10.1021/ja902087t)
- [29] L. Anfossi, S. Cavalera, F. Di Nardo, G. Spano, C. Giovannoli, C. Baggiani, Delayed addition of template molecules enhances the binding properties of diclofenac-imprinted polymers. *Polymers* 12 (2020) 1178. doi:[10.3390/polym12051178](https://doi.org/10.3390/polym12051178)
- [30] B. Sellergren, The non-covalent approach to molecular imprinting. In: B. Sellergren (ed.): *Molecularly Imprinted Polymers. Man-made Mimics of Antibodies and their Applications in Analytical Chemistry*. Elsevier, Amsterdam. (2001) Chap. 5, pp. 138–179.
- [31] B. Sellergren, A.J. Hall, Fundamental aspects on the synthesis and characterisation of imprinted network polymers. In: B. Sellergren (ed.): *Molecularly Imprinted Polymers. Man-made Mimics of Antibodies and their Applications in Analytical Chemistry*. Elsevier, Amsterdam. (2001) Chap. 2, pp. 29–35.
- [32] M.M. Sanagi, S. Salleh, W.A.W. Ibrahim, A.A. Naim, D. Hermawan, M. Miskam, I. Hussain, H.Y. Aboul-Enein, Molecularly imprinted polymer solid-phase extraction for the analysis of organophosphorus pesticides in fruit samples. *J. Food Composition Anal.* 32 (2013) 155–161. doi:[10.1016/j.jfca.2013.09.001](https://doi.org/10.1016/j.jfca.2013.09.001)
- [33] Ç. Öter, Ö.S. Zorer, Molecularly imprinted polymer synthesis and selective solid phase extraction applications for the detection of ziram, a dithiocarbamate fungicide. *Chem. Eng. J. Adv.* 7 (2021) 100118. doi:[10.1016/j.ceja.2021.100118](https://doi.org/10.1016/j.ceja.2021.100118)

## SUPPORTING INFORMATION

### Development of molecularly imprinted polymer for the selective recognition of the weakly interacting fenamiphos molecule

Chaima Nasraoui<sup>1,3</sup>, Najeh Jaoued-Grayaa<sup>2</sup>, Laurent Vanoye<sup>4</sup>, Yves Chevalier<sup>3,\*</sup> and Souhaira Hbaieb<sup>1,\*</sup>

1- *Laboratoire de Recherche: Caractérisations, Applications et Modélisation de Matériaux, Université de Tunis El Manar, Faculté des Sciences de Tunis, Université El Manar, Tunisia.*

2- *Unité Spécialisée de développement des techniques analytiques, Institut National de Recherche et d'Analyse Physico-chimique, Biotechpole Sidi-Thabet, 2020 Ariana, Tunisia.*

3- *Laboratoire d'Automatique, de Génie des Procédés et de Génie Pharmaceutique, Université de Lyon 1, UMR 5007 CNRS, 43 bd 11 Novembre, 69622 Villeurbanne, France.*

4- *Catalyse, Polymérisation, Procédés et Matériaux, CP2M, Université de Lyon 1, CPE Lyon, UMR 5128 CNRS, 43 bd 11 Novembre, 69622 Villeurbanne, France.*

#### SI1. Grafting of MPTMS onto silica nanoparticles

In order to ensure successful polymerization on the surface of the support material in the process of surface imprinting, fumed silica surface was functionalized to allow a covalent attachment of the MIP to the silica surface. The mercaptosilane coupling agent was covalently bound to the silica surface by a direct condensation reaction of surface silanols with the methoxy groups of 3-MPTMS according to the anhydrous process. Such process allows binding a dense monolayer at the surface of silica. The thiol groups of 3-MPTMS have strong radical transfer reactivity and can effectively participate to the polymerization by means of a radical transfer reaction. The resulting SiO<sub>2</sub>-MPTMS particles were characterized by IR spectroscopy, Raman scattering, <sup>13</sup>C CP-MAS NMR, thermogravimetric analysis and sulfur elemental analysis.

IR spectra of fumed silica and modified silica presented in [Fig. S1](#) show the characteristic bands of silica network, a sharp and strong absorption at 1010–1190 cm<sup>-1</sup> and a weaker band at 800–900 cm<sup>-1</sup> correspond to the Si–O–Si stretching, indicating that there is no significant change in the main silica structure by surface modification. In modified silica spectrum, supplementary bands were observed at 2928–2858 cm<sup>-1</sup> ascribed to the symmetric and asymmetric stretching of –CH<sub>2</sub> and a weak band at 2575 cm<sup>-1</sup> related to stretching vibrations of the S–H group [1]. It indicates that the alkyl chain of 3-MPTMS has been grafted onto nano-silica surface. The broad band located in the range 3000–4000 cm<sup>-1</sup> corresponds to O–H stretching vibrations of surface silanol groups. In

bare silica spectra, this band is broad because the surface density of Si–OH is higher leading to rising hydrogen-bonded O–H groups. However, for modified silica, this band has been considerably sharpened and shifted to a higher wavenumber (Fig. S1). This indicates that a significant part of the Si–OH groups was isolated due to the grafting reaction. The –SH group band corresponding to the grafting 3-MPTMS molecules was very weak due to the strong vibration of silica which overlaps vibrations of 3-MPTMS functional groups. The S–H stretching vibration is more intense in Raman spectroscopy and appears at 2576  $\text{cm}^{-1}$  (Fig. S2).

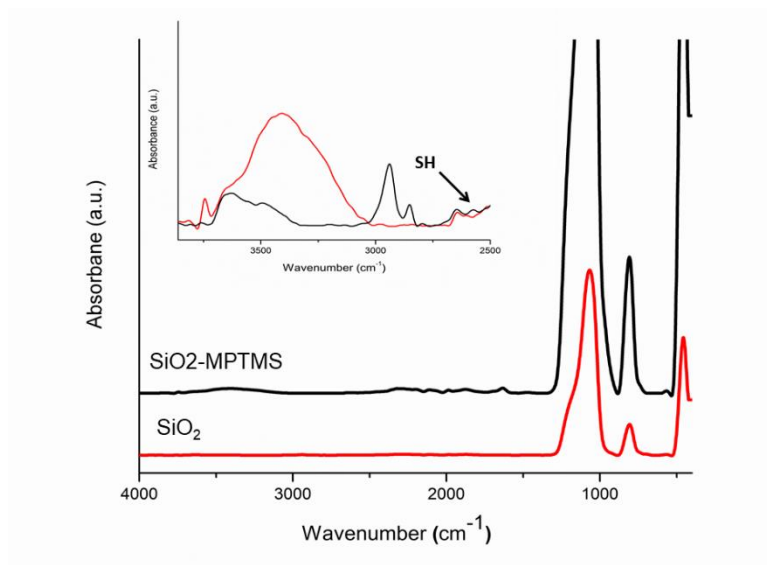


**Figure S1.** IR spectra of unmodified and MPTMS-grafted SiO<sub>2</sub> particles.

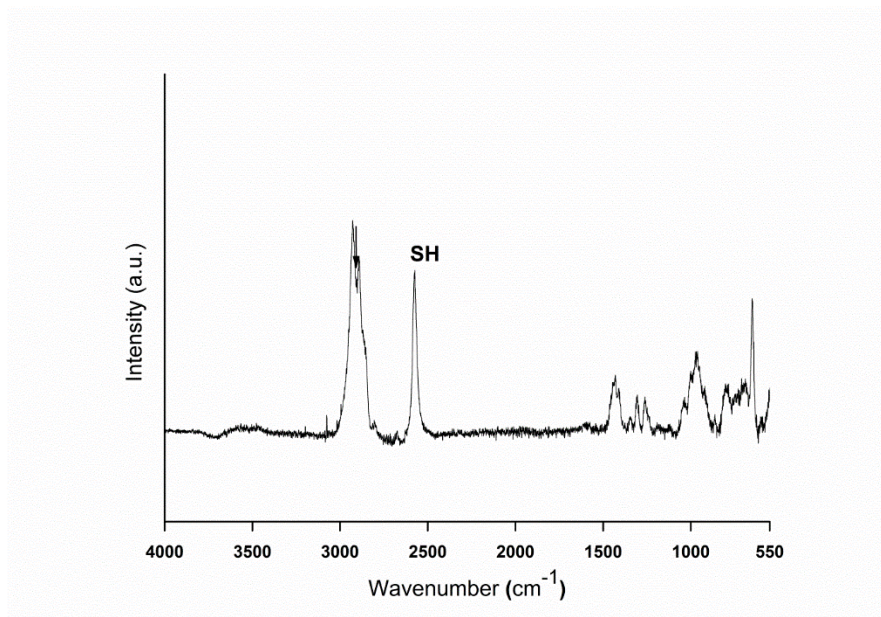


**Figure S2.** Raman spectrum of SiO<sub>2</sub>-MPTMS.

The  $^{13}\text{C}$  CP-MAS NMR spectrum of modified silica (Fig. S3) exhibits the signals of carbons belonging to 3-MPTMS moieties. The lines at 14 ppm, 29 ppm and 50 ppm are respectively assigned to the methylene group directly linked to the silicon atom ( $\text{Si}-\text{CH}_2-$ ), the two other methylene groups ( $-\text{CH}_2-\text{CH}_2-\text{SH}$ ), and residual  $\text{Si}-\text{OCH}_3$  resulting from the incomplete condensation reaction of methoxy groups. This result clearly confirms the grafting of 3-MPTMS onto the silica surface.

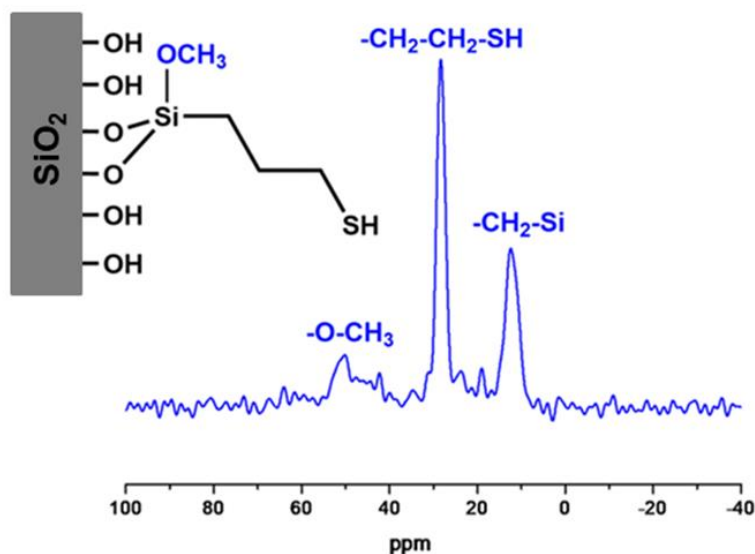


**Figure S3.**  $^{13}\text{C}$  CP-MAS NMR spectrum of  $\text{SiO}_2$ -MPTMS.

Thermogravimetric analysis (TGA) was used to determine the amount of silane chains grafted onto the silica surface per unit area. The TGA curve of modified silica (Fig. 6) presents a sharp mass loss beginning at 250 °C and continuing till 700 °C. It is attributed to the thermal decomposition of 3-MPTMS chains. The grafting density was estimated from the recorded mass loss of 3-MPTMS (7.0 %) and the molar mass of the lost organic moiety  $-(\text{CH}_2)_3-\text{SH}$  of  $75 \text{ g}\cdot\text{mol}^{-1}$  as follows:

$$\text{Grafting density } (\text{mol}\cdot\text{m}^{-2}) = \frac{\% \text{mass loss}}{100 \times 75 \times A_{\text{sp}}} \quad (\text{S1})$$

where  $A_{\text{sp}} = 200 \text{ m}^2\cdot\text{g}^{-1}$  is the specific area of raw fumed silica.

The grafting density of 3-MPTMS on silica surface was  $4.7 \mu\text{mol}\cdot\text{m}^{-2}$  and it was in good accordance with the value inferred from the elemental analyses of sulfur (%S = 3.1 %) using the following equation:

$$\text{Surface density (mol}\cdot\text{m}^{-2}) = \frac{\%S}{100 \times 32.065 \times A_{\text{SP}}} \quad (\text{S2})$$

The grafting density was close to the maximum grafting density of a dense close-packed monolayer of organosilane ( $2\text{--}4 \mu\text{mol}\cdot\text{m}^{-2}$ ). Higher coverage value could lead to multilayer coating made of oligomeric species of 3-MPTMS attached to the silica surface. This would result in a thicker and inhomogeneous layer.

## SI2. Characterization of molecularly imprinted polymers

The IR spectra of MIP/2-METAC and NIP/2-METAC (Fig. S4a) showed the characteristic absorption bands of the quaternary ammonium group ( $-\text{N}^+(\text{CH}_3)_3$ ) and  $-\text{C}-\text{N}$  moiety at  $1485 \text{ cm}^{-1}$  and  $1240 \text{ cm}^{-1}$  respectively. The bands at  $2900 \text{ cm}^{-1}$  and  $1720 \text{ cm}^{-1}$  were assigned to ( $-\text{CH}$ ) and ( $-\text{C}=\text{O}$ ) groups respectively. This result confirmed the incorporation of 2-METAC and the cross-linking agent in the polymer backbone.

The IR spectra of MIP/4-VP and NIP/4-VP (Fig. S4b) show the characteristic absorption bands of 4-VP appearing at  $1637$  and  $1450 \text{ cm}^{-1}$  related to the  $\text{C}=\text{N}$  and  $\text{C}=\text{C}$  stretching vibrations of the pyridine ring. The band at  $1720 \text{ cm}^{-1}$  is due to the  $\text{C}=\text{O}$  stretching vibration of EDGMA. These results indicated that the 4-VP and EDGMA have been successfully copolymerized on the surface of modified silica.

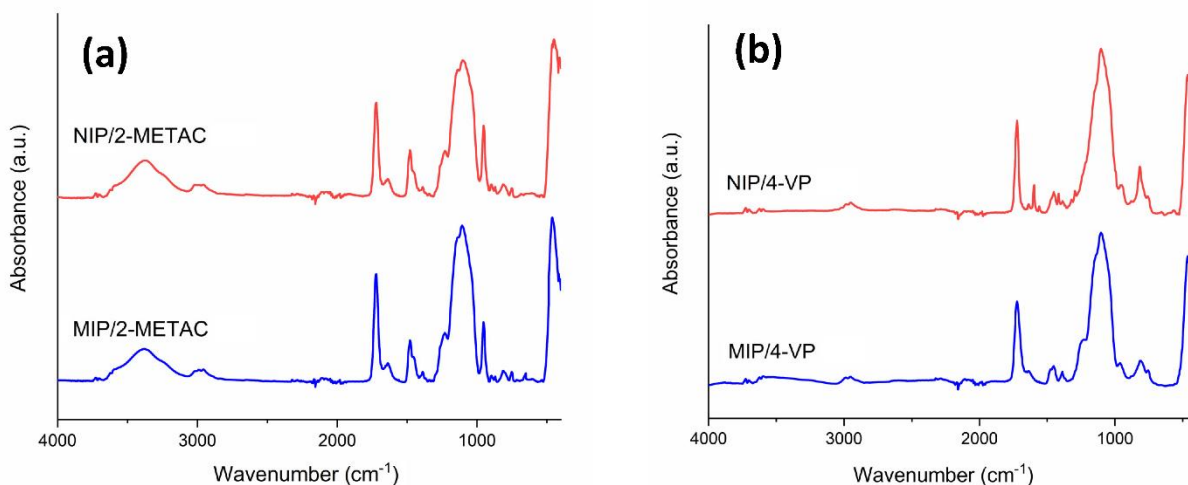


**Figure S4.** IR spectra of: (a) MIP/2-METAC and NIP/2-METAC, (b) MIP/4-VP and NIP/4-VP.

The  $^{13}\text{C}$  CP/MAS NMR spectrum of MIP/2-METAC depicts signals of methyl, methylene, aliphatic and carbonyl groups at 4.57 ppm, 46.43 ppm, 31.53 ppm and 164.04 ppm respectively. In the spectrum of MIP/4-VP, these signals were shifted to 4.52 ppm, 48.39 ppm, 31.57 ppm and 163.51 ppm (Fig. S5). The variation of chemical shift was larger in the case of methylene and carbonyl groups which can be explained by the change in chemical environment resulted from the variation of monomer type.

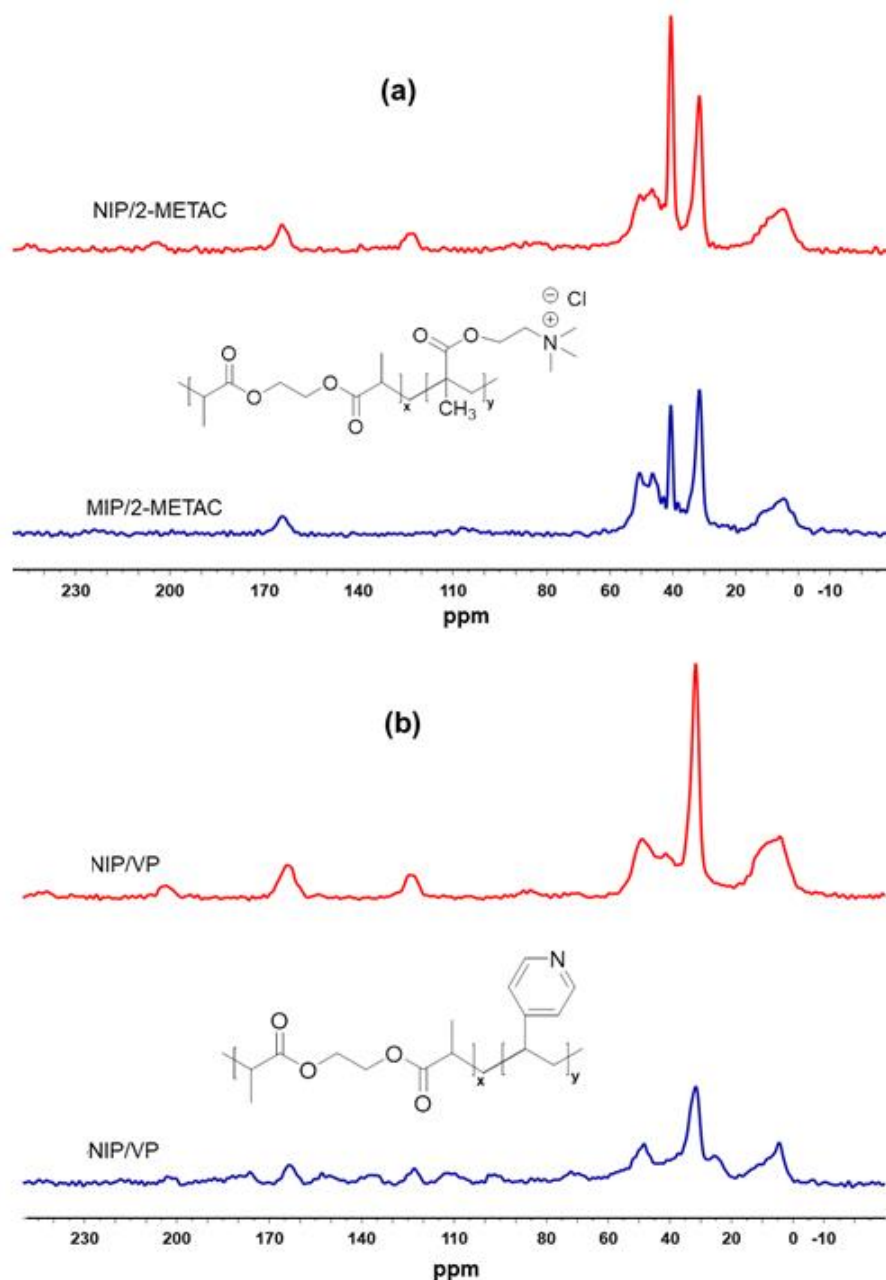


**Figure S5.** Solid-state  $^{13}\text{C}$  CP/MAS NMR spectra of the materials: (a) MIP/2-METAC and NIP/2-METAC (b) MIP/4-VP and NIP/4-VP.

The TGA records of MIP/2-METAC, NIP/2-METAC, MIP/4-VP and NIP/4-VP (Fig. S6) show the same features as that of MIP/MAA and NIP/MAA (Fig. 5).

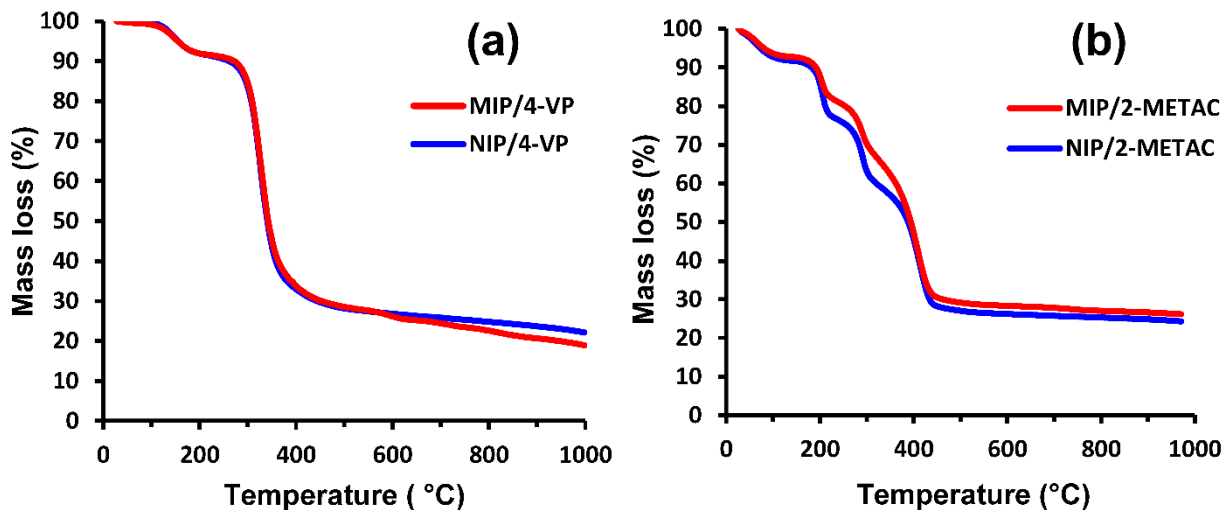


**Figure S6.** Thermogravimetric analysis of the samples: (a) MIP/4-VP and NIP/4-VP, (b) MIP/2-METAC and NIP/2-METAC.

### SI3. NMR titration study

The protons of fenamiphos observed in NMR are illustrated in Figure S7.

The experimental data of fenamiphos  $^1\text{H}$  and  $^{31}\text{P}$  chemical shift changes as a function of [monomer]/[fenamiphos] is depicted in Figures S8, S9 and S10, together with the best fit of the model for 1:1 association to the experimental data.

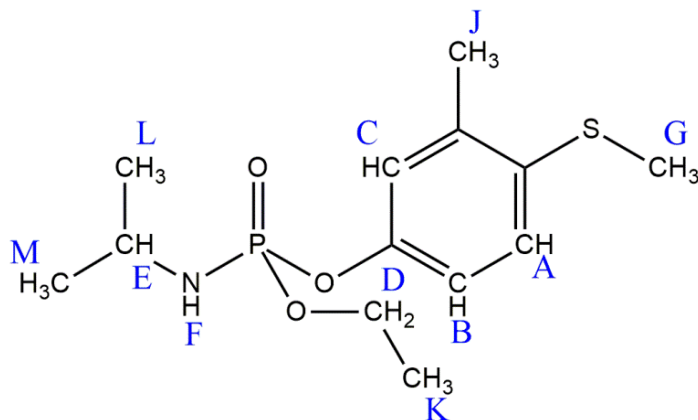


**Figure S7.** Fenamiphos protons studied by  $^1\text{H}$  NMR.

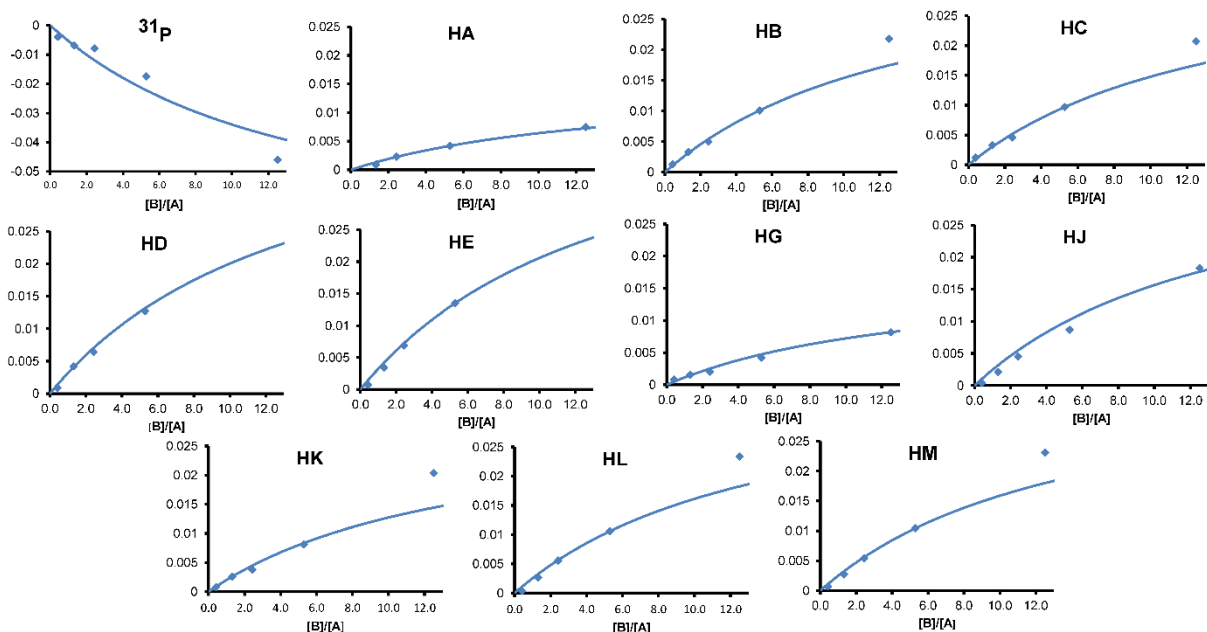


**Figure S8.** Plots of experimental and non-linear fits of fenamiphos  $^{31}\text{P}$  and  $^1\text{H}$  chemical shifts variations  $\Delta\delta$ (ppm) with respect to free fenamiphos as a function of  $[\text{B}]/[\text{A}] = [\text{MAA}]/[\text{fenamiphos}]$ .

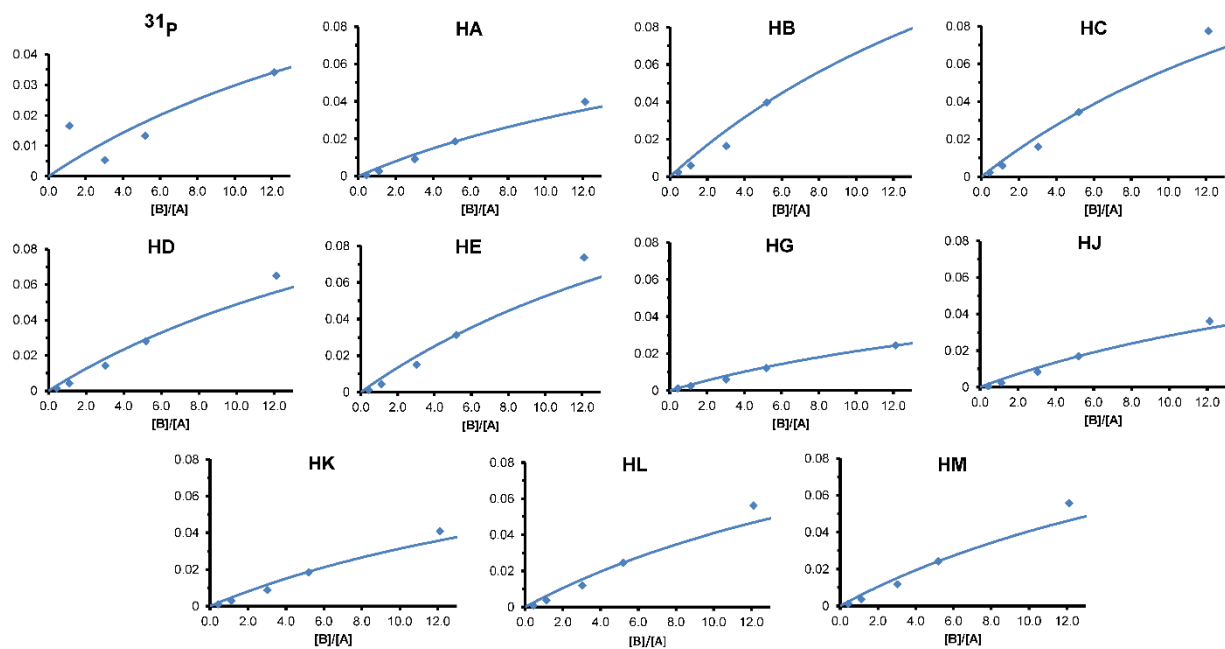


**Figure S9.** Plots of experimental and non-linear fits of fenamiphos  $^{31}\text{P}$  and  $^1\text{H}$  chemical shifts variations  $\Delta\delta$ (ppm) with respect to free fenamiphos as a function of  $[\text{B}]/[\text{A}] = [4\text{-VP}]/[\text{fenamiphos}]$ .

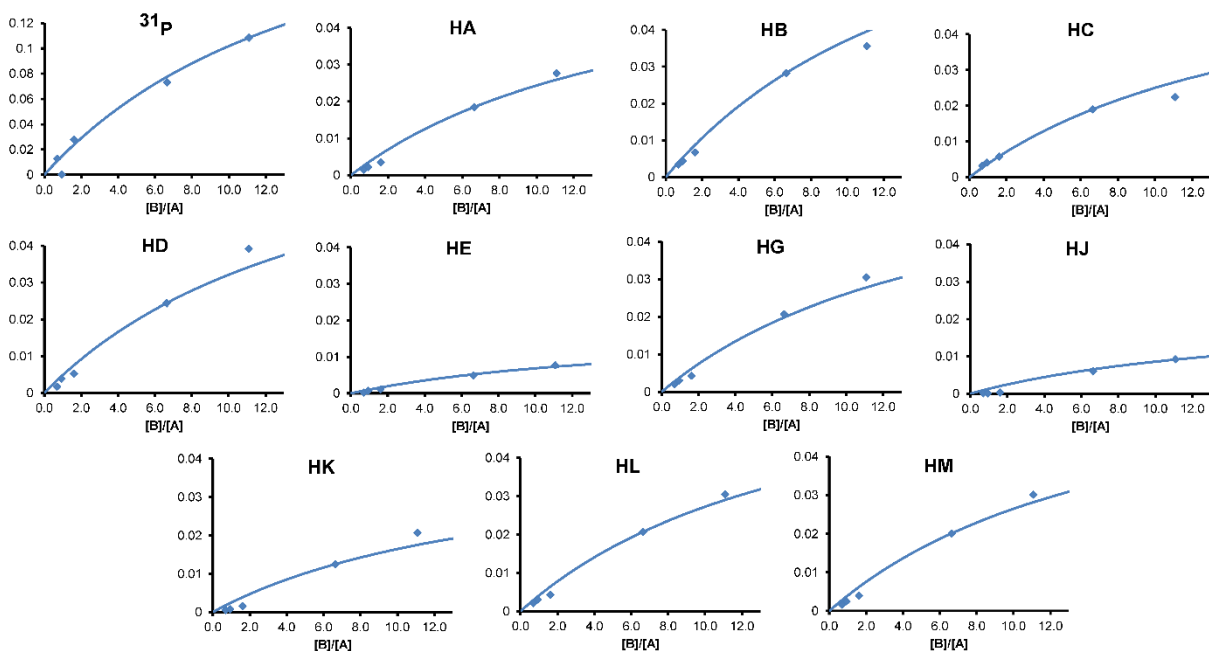


**Figure S10.** Plots of experimental and non-linear fits of fenamiphos  $^{31}\text{P}$  and  $^1\text{H}$  chemical shifts variations  $\Delta\delta$ (ppm) with respect to free fenamiphos as a function of  $[\text{B}]/[\text{A}] = [\text{2-METAC}]/[\text{fenamiphos}]$ .

## References

- [1] G. Socrates, *Infrared and Raman Characteristic Group Frequencies*. 3<sup>rd</sup> ed., Wiley, Chichester (2001) p. 209.
- [2] A. Anene, R. Kalfat, Y. Chevalier, S. Hbaieb, Design of molecularly imprinted polymeric materials: The crucial choice of functional monomers. *Chem. Africa* 3 (2020) 769–781. doi: [10.1007/s42250-020-00180-1](https://doi.org/10.1007/s42250-020-00180-1)